The Astrophysical Journal, 889:25 (16pp), 2020 January 20 https://doi.org/10.3847/1538-4357/ab61f1


# OGLE-ing the Magellanic System: Cepheids in the Bridge*

Anna M. Jacyszyn-Dobrzeniecka[1,2], Igor Soszyński[1], Andrzej Udalski[1], Michał K. Szymański[1], Dorota M. Skowron[1], Jan Skowron[1], Przemek Mróz[1,5], Katarzyna Kruszyńska[1], Patryk Iwanek[1], Paweł Pietrukowicz[1], Radosław Poleski[3], Szymon Kozłowski[1], Krzysztof Ulaczyk[4], Krzysztof Rybicki[1], and Marcin Wrona[1]
[1] Astronomical Observatory, University of Warsaw, Al. Ujazdowskie 4, 00-478 Warszawa, Poland; jacyszyn@uni-heidelberg.de
[2] Astronomisches Rechen-Institut, Zentrum für Astronomie der Universität Heidelberg, Mönchhofstr. 12-14, D-69120 Heidelberg, Germany
[3] Department of Astronomy, Ohio State University, 140 West 18th Avenue, Columbus, OH 43210, USA
[4] Department of Physics, University of Warwick, Coventry CV4 7AL, UK
[5] Division of Physics, Mathematics, and Astronomy, California Institute of Technology, Pasadena, CA 91125, USA
*Received 2019 April 18; revised 2019 December 5; accepted 2019 December 8; published 2020 January 22*

## Abstract

We present a detailed analysis of the Magellanic Bridge Cepheid sample constructed using the Optical Gravitational Lensing Experiment Collection of Variable Stars. Our updated Bridge sample contains 10 classical and 13 anomalous Cepheids. We calculate their individual distances using optical period–Wesenheit relations and construct three-dimensional maps. Classical Cepheid (CC) on-sky locations match very well neutral hydrogen and young stars distributions; thus, they add to the overall young Bridge population. In three dimensions, 8 out of 10 CCs form a bridge-like connection between the Magellanic Clouds. The other two are located slightly farther away and may constitute the Counter Bridge. We estimate ages of our Cepheids to be less than 300 Myr for from 5 up to 8 out of 10, depending on whether the rotation is included. This is in agreement with a scenario where these stars were formed in situ after the last encounter of the Magellanic Clouds. Cepheids' proper motions reveal that they are moving away from both Large and Small Magellanic Clouds. Anomalous Cepheids are more spread than CCs in both two and three dimensions, even though they form a rather smooth connection between the Magellanic Clouds. However, this connection does not seem to be bridge-like, as there are many outliers around both Magellanic Clouds.

*Unified Astronomy Thesaurus concepts:* Magellanic Clouds (990); Cepheid variable stars (218)

## 1. Introduction

The Magellanic Bridge (MBR), which undoubtedly is direct evidence of the Magellanic Clouds' interactions, has been a subject of interest of many research projects. Though observations of the Bridge area started with Shapley's first discovery of young stars located in the SMC Wing (Shapley 1940), the Bridge as a structure was discovered as a hydrogen feature (Hindman et al. 1963). Numerical models predict that the connection between the Large and Small Magellanic Clouds (LMC and SMC, respectively) was formed after their last encounter, about 200–300 Myr ago (e.g., Gardiner et al. 1994; Gardiner & Noguchi 1996; Růžička et al. 2010; Besla et al. 2012; Diaz & Bekki 2012) or, as recent study shows, slightly later—about 150 Myr ago (Zivick et al. 2019).

Different studies of the gaseous counterpart of the MBR showed that it is a rather complicated, multiphase structure (D'Onghia & Fox 2016 and references therein). The neutral hydrogen (H I) kinematics reveal that the Bridge is connected with the western parts of the LMC disk (Indu & Subramaniam 2015) and, moreover, is also being sheared. Other studies showed that the Bridge also contains warm ionized gas (Barger et al. 2013). Moreover, Wagner-Kaiser & Sarajedini (2017) found evidence of dust in the MBR, concluding that it has probably been pulled out of either or both Magellanic Clouds during their interactions.

Here we present a detailed analysis of classical and anomalous Cepheids in the Bridge area. Different stellar components of the Bridge have been discovered. This is in agreement with numerical model predictions (e.g., Besla et al. 2012; Diaz & Bekki 2012; Guglielmo et al. 2014). Many studies were devoted to searching for young stars between the Magellanic Clouds and found evidence of their presence therein (Shapley 1940; Irwin et al. 1985; Demers & Battinelli 1998; Harris 2007; Noël et al. 2013, 2015; Skowron et al. 2014; Belokurov et al. 2017; Mackey et al. 2017; Zivick et al. 2019). Skowron et al. (2014) showed, using the Optical Gravitational Lensing Experiment (OGLE) data, that young stars form a continuous bridge-like connection and that their distribution is clumped. This was confirmed by Belokurov et al. (2017), who tested young main-sequence stars from *Gaia* and *GALEX*, as well as Mackey et al. (2017), who used Dark Energy Camera data. Young ages of some of these stars strongly suggest an in situ formation. Zivick et al. (2019) found a correlation between the young population and H I. Moreover, studies of stellar proper motions (PMs) for both young and old populations (Oey et al. 2018; Zivick et al. 2019) show that the Bridge is moving away from the SMC and toward the LMC.

The clumped pattern of stellar associations' distribution between the Magellanic Clouds may suggest an ongoing process of forming a tidal dwarf galaxy (Bica & Schmitt 1995; Ploeckinger et al. 2014, 2015, 2018; Bica et al. 2015). Recently, a dwarf galaxy was found located in the on-sky Bridge area, though it is located halfway between the Sun and the Magellanic System (Koposov et al. 2018).

Classical pulsators were also studied in the MBR. Soszyński et al. (2015b), as part of the OGLE Collection of Variable Stars (OCVS), published a list of classical Cepheids (CCs), including new discoveries located in the MBR. Jacyszyn-Dobrzeniecka et al. (2016, hereafter Paper I) studied their three-dimensional distribution and classified nine as MBR members. Five of these

* Draft version prepared on 2019 December 5.

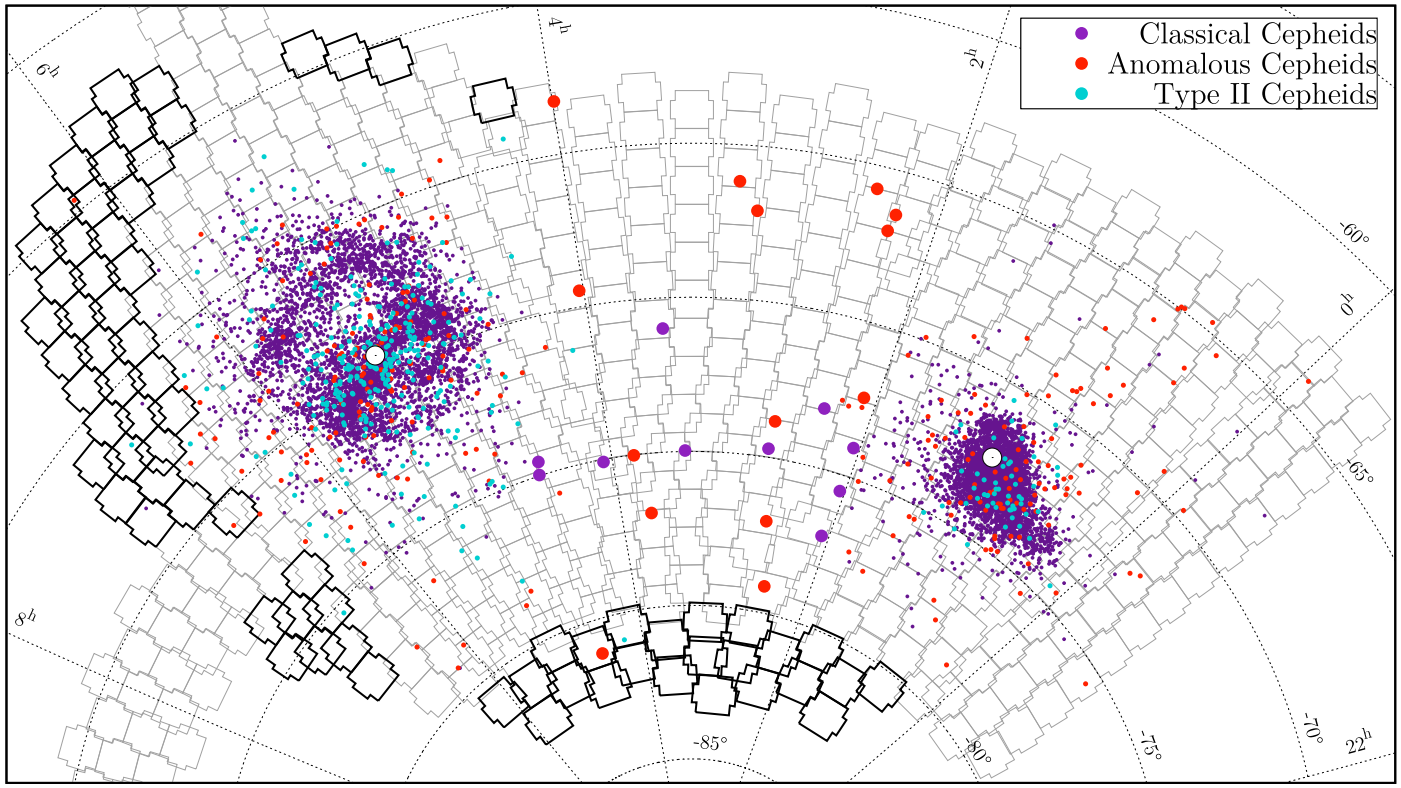


**Figure 1.** On-sky locations of Cepheids in the Magellanic System. The selected Bridge sample is featured with larger circles. Black contours show the newest addition to the OGLE-IV fields, while gray contours show main OGLE-IV fields in the Magellanic System that were already observed before 2017 July. White circles mark the LMC (van der Marel & Kallivayalil 2014) and SMC (Stanimirović et al. 2004) centers.

objects seem to form a bridge-like connection between the Magellanic Clouds, while the others are more spread in three dimensions. Ages of these CCs suggest that they were formed in situ, as almost all are under 300 Myr.

The evidence was found for intermediate-age and old stars between the Magellanic Clouds (Bagheri et al. 2013; Noël et al. 2013, 2015; Skowron et al. 2014; Carrera et al. 2017). Classical pulsators belonging to the latter group, the RR Lyrae stars, are also present in the MBR, and their distribution was thoroughly tested (Jacyszyn-Dobrzeniecka et al. 2017, hereafter Paper II; Belokurov et al. 2017; Wagner-Kaiser & Sarajedini 2017). Also Mira candidates were searched for in the MBR (Deason et al. 2017). Another paper in the series of using OCVS to analyze the three-dimensional structure of the Magellanic System (Jacyszyn-Dobrzeniecka et al. 2020, hereafter Paper IV), following closely this paper, summarizes and updates the current knowledge of RR Lyrae stars' distribution in the Bridge. For more information on the old stellar counterpart of the MBR, see the Introduction in Paper IV.

In this work we present an analysis of Cepheids in the MBR using the updated, corrected, and extended OGLE data. We studied three-dimensional distributions of CCs, anomalous Cepheids (ACs), and type II Cepheids (T2Cs), though we did not classify any of the latter as MBR members. For CCs and ACs we also present a detailed analysis of many parameters and a comparison of different methods used. In this paper we also compare our sample to *Gaia* Data Release 2 (DR2) Cepheids and for the first time present their distribution in the Bridge.

We organized the paper as follows. In Section 2 we present the OCVS, as well as the latest changes and updates applied to the collection. Section 3 presents methods of calculating individual distances and coordinates' transformation. A detailed analysis of CC and AC distributions is included in Sections 4 and 5, respectively. In Section 6 we discuss the influence of the recent reclassification of four Cepheids on their parameters. For the first time we present *Gaia* DR2 Cepheids in the Bridge and compare them to the OCVS Cepheids in Section 7. We summarize and conclude the paper in Section 8.

## 2. Observational Data

### 2.1. OGLE Collection of Variable Stars

In this study we use data from the fourth phase of the OGLE project (Udalski et al. 2015). In particular, we use Cepheids from the OCVS in the Magellanic System (Soszyński et al. 2015b, 2017), including the latest updates (Soszyński et al. 2019). Most of the updates come from the newly added OGLE fields that are marked with black contours in Figure 1. Moreover, the updates also concerned a reclassification of types and modes of pulsation for four Cepheids from the MBR area that were presented in Paper I. This is due to their light-curve Fourier decomposition parameters suggesting different classification (Soszyński et al. 2015a). One Cepheid was moved from first-overtone to fundamental-mode CC. Three CCs were reclassified as ACs.

For one CC in our sample, namely, OGLE-SMC-CEP-4986, the *V*-band magnitude was not available in the OGLE database. Thus, we used the ASAS-SN Sky Patrol light curve (Schappee et al. 2014; Kochanek et al. 2017) to calculate its mean magnitude in the *V* band. To make sure it is properly calibrated, we selected 10 reference stars located in the same detector (OGLE operates a 32-chip mosaic camera) as the Cepheid. These objects were nonvariables and had the closest magnitude and color to OGLE-SMC-CEP-4986, as well as good-quality

magnitude measurement in the OGLE database (many epochs). For the reference stars we compared magnitudes in the OGLE and ASAS-SN Sky Patrol and calculated a correction, which was on the order of 0.08 mag.

## 3. Data Analysis

### 3.1. Period–Luminosity Relations and Individual Distances

To calculate individual distances of Cepheids, we used the entire Magellanic System samples and applied the same technique as in Paper I (see Section 3.1 therein for more details). We did this separately for CCs and ACs. Using Wesenheit magnitudes (Madore 1982), we fitted period–luminosity (PL) relations (Leavitt law) to the LMC sample (see Equations (1) and (2) in Paper I). Together with the least-squares method, we applied $3\sigma$ clipping to the data. We note, however, that this approach may not be the most appropriate for studying distances (Deb et al. 2018), as Nikolaev et al. (2004) showed that the error distribution is not normal for Wesenheit index at a given period. On the other hand, many studies proved this technique to be very robust in the case of the Magellanic System (e.g., Haschke et al. 2012a, 2012b; Moretti et al. 2014; Paper I; Inno et al. 2016; Ripepi et al. 2017).

For fundamental-mode CCs we included a break in the PL relation at $\log P = 0.4$. For first-overtone CCs we excluded objects with $\log P < -0.3$ (see Section 3.1 in Paper I and Soszyński et al. 2008). Figure 2 shows separate PL relations for the final LMC and SMC CC and AC samples with Bridge Cepheids overplotted on each panel using larger symbols. Each type and mode is plotted using a different point type. Additionally, the bottom row highlights the four reclassified Cepheids and shows their local IDs (labels consisting of an "M" with a number that we started using in Paper I). The parameters of our fits are consistent with those from Paper I and are shown in Table 1. The number of stars included in the fits is slightly smaller than in Paper I because this time we did not complement our final set with OGLE-III observations.

We then followed our previous technique as described in detail in Section 3.2 of Paper I. We assumed that the fitted PL relation corresponds to the mean LMC distance and the individual distances were calculated with respect to the best fit (see Equations (3), (4), (5) in Paper I). As a reference distance we have used the most accurate up-to-date result obtained by Pietrzyński et al. (2019). The resulting three-dimensional distribution of CCs is discussed in the next section.

### 3.2. Coordinate Transformations

In this study we again use Hammer equal-area sky projection as we did in Papers I and II. The projection is rotated so that the $z$-axis is pointing toward $\alpha_{\rm cen} = 3^{\rm h}20^{\rm m}$, $\delta_{\rm cen} = -72°$. This time we have introduced one small correction to Equations (7)–(11) from Paper I that leads to a coordinate system with an $x$-axis that is symmetrical with respect to $\alpha_{\rm cen}$. We have also added a coefficient of $-\frac{\pi}{2}$ when normalizing $l$ that was missing in our original equations:

$$\alpha_{\rm b} = \alpha + \left(\frac{\pi}{2} - \alpha_{\rm cen}\right) \tag{1}$$

$$l = \arctan\left(\frac{\sin(\alpha_{\rm b})\cos(\delta_{\rm cen}) + \tan(\delta)\sin(\delta_{\rm cen})}{\cos(\alpha_{\rm b})}\right) \tag{2}$$

$$\beta = \arcsin(\sin(\delta)\cos(\delta_{\rm cen}) - \cos(\delta)\sin(\delta_{\rm cen})\sin(\alpha_{\rm b})), \tag{3}$$

where $l$ and $\beta$ are auxiliary variables. We normalize the coordinates so that $l - \frac{\pi}{2} \in (-\pi, \pi)$ and $\beta \in \left(-\frac{\pi}{2}, \frac{\pi}{2}\right)$:

$$x_{\rm Hammer} = -\frac{2\sqrt{2}\cos(\beta)\sin(l/2)}{\sqrt{1 + \cos(\beta)\cos(l/2)}} \tag{4}$$

$$y_{\rm Hammer} = \frac{\sqrt{2}\sin(\beta)}{\sqrt{1 + \cos(\beta)\cos(l/2)}}. \tag{5}$$

## 4. Classical Cepheids

### 4.1. Updated Bridge Sample

In this section we present a detailed analysis of the updated sample of CCs in the Magellanic System in the context of the MBR. The sample of Bridge CCs was first presented by Soszyński et al. (2015b) and included five objects. Later, in Paper I we have enlarged that sample to nine and discussed their three-dimensional locations in detail (see Section 6 therein). We labeled the objects M1–M9 (see Table 10 in Paper I). Since then, Soszyński et al. (2017) have already added one classical Cepheid to the OGLE Bridge sample, making it the 10th one (M10).

Later, Soszyński et al. (2019) reclassified M7 from first-overtone CC to fundamental-mode CC. Moreover, three objects were moved from the CC sample to the AC sample, namely, M2, M3, and M8. The applied corrections influenced Cepheids' distances, decreasing them by even up to ∼20 kpc. Thus, the three-dimensional distribution of the Bridge sample has significantly changed as compared to Paper I.

We have constructed our final Bridge Cepheid sample based on the on-sky and three-dimensional locations of Cepheids in relation to the LMC and SMC entire samples. We decided to add two objects located close to the LMC (M12 and M13) to the Bridge sample. These CCs were already included in the first OGLE-IV Collection of CCs by Soszyński et al. (2015b) as LMC stars, though we did not incorporate these in the Paper I sample. All of the four outlier Cepheids, located both on the SMC side (M9 and M11; M11 was added by Soszyński et al. 2017 and was not present in the Paper I sample) and on the LMC side (M12, M13), are connecting the Clouds' samples to the genuine MBR sample.

Due to these updates and corrections, our final Bridge CC sample consists of 10 objects. The list of CCs and their basic parameters is included in Table 2, which provides the object's OCVS ID, local ID used in Paper I and this work, pulsation period $P$, mean magnitudes from both OGLE passbands ($I$ and $V$), R.A. and decl. (epoch J2000.0), distance $d$ (details on the method used—see Section 3.1), and age estimated using the period–age relation from Anderson et al. (2016) (including average rotation) and Bono et al. (2005) (without rotation). The list comprises five fundamental-mode pulsators, four first-overtone pulsators, and one double-mode Cepheid (pulsating simultaneously in the first and second overtone), for which we used its first-overtone period in this analysis.

Our Bridge Cepheid sample also consists of ACs that we discuss in Section 5. We note that we did not classify any of the recently published T2Cs in the Magellanic System (Soszyński et al. 2018) as a Bridge candidate, as these stars do not seem to form any bridge-like connection and none are located in the direct area of interest.

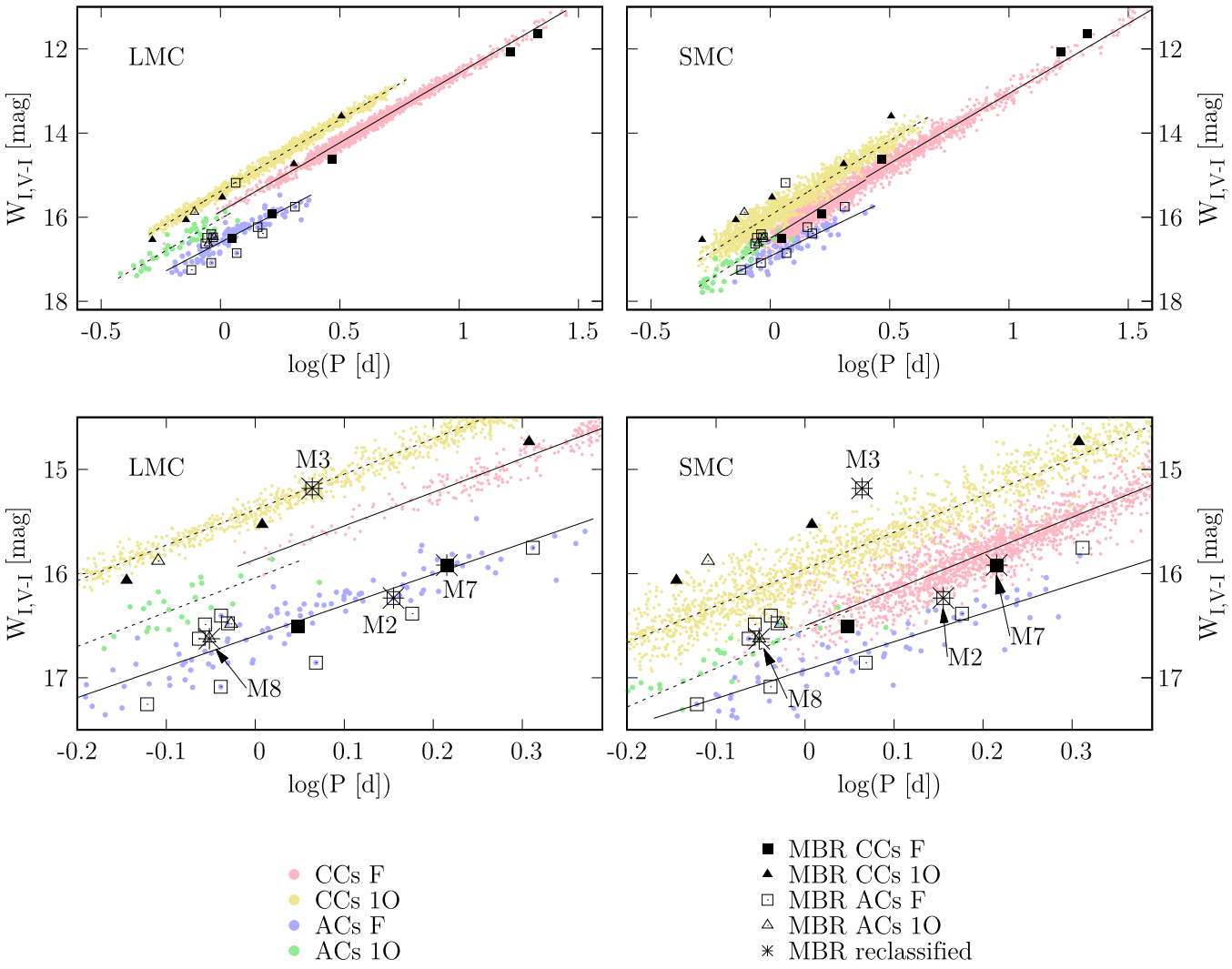


**Figure 2.** PL relations for classical and anomalous Cepheids in the LMC (left column) and SMC (right column). CCs are marked with smaller circles than ACs. The entire Bridge sample is overplotted on the presented PL relations in every panel, with each type marked separately. Additionally, bottom panels highlight four Cepheids that were reclassified and are marked with a star and their local ID. M7 was reclassified from first-overtone CC to fundamental-mode CC; M2 and M3, from fundamental-mode CCs to fundamental-mode ACs; and M8, from first-overtone CC to first-overtone AC. Plots do not show $3\sigma$ outliers, as these were removed from the final sample. The fit for fundamental-mode ACs in the SMC has significantly different slope than all of the other relations. Note, however, that we do not use the SMC AC PL relations and that these are only plotted here for comparison.

**Table 1**
PL Relations for CCs in the Magellanic System in the Wesenheit Magnitude

| $W_{I,V-I} = a \log P + b$ | | | | | | | | |
|---|---|---|---|---|---|---|---|---|
| Galaxy | Puls. Mode | $\log P$ | $a$ | $b$ (mag) | $\sigma$ (mag) | $\chi^2$/dof | $N_{\rm inc}$ | $N_{\rm rej}$ |
| LMC | F | $\leqslant$0.4 | $-3.234 \pm 0.033$ | $15.866 \pm 0.010$ | 0.104 | 3.029 | 273 | 6 |
| | | >0.4 | $-3.315 \pm 0.008$ | $15.888 \pm 0.005$ | 0.076 | 1.613 | 2042 | 85 |
| | | all | $-3.311 \pm 0.006$ | $15.885 \pm 0.004$ | 0.079 | 1.714 | 2308 | 98 |
| | 1O | all | $-3.411 \pm 0.007$ | $15.387 \pm 0.003$ | 0.077 | 1.634 | 1772 | 85 |
| SMC | F | $\leqslant$0.4 | $-3.470 \pm 0.015$ | $16.501 \pm 0.004$ | 0.162 | 7.362 | 1698 | 38 |
| | | >0.4 | $-3.330 \pm 0.008$ | $16.389 \pm 0.006$ | 0.149 | 6.170 | 935 | 28 |
| | | all | $-3.453 \pm 0.005$ | $16.489 \pm 0.002$ | 0.159 | 7.106 | 2636 | 63 |
| | 1O | all | $-3.535 \pm 0.007$ | $15.957 \pm 0.002$ | 0.171 | 8.198 | 1879 | 30 |

**Note.** $N_{\rm inc}$ is the number of objects included in the fit, while $N_{\rm rej}$ is the number of objects rejected during the $3\sigma$-clipping procedure.

It is noteworthy, however, that Iwanek et al. (2018) studied three-dimensional distributions of ACs and T2Cs in the context of the stellar evolution theory. They found that T2Cs are probably members of old and intermediate-age populations, while ACs seem to belong to the old population as is demonstrated by their spread on-sky view.

In Figure 3 we compare the on-sky distribution of different tracers in the central Bridge area. The plot shows classical

**Table 2**
Magellanic Bridge Classical Cepheids: Basic Parameters

| Mode | OCVS ID / Loc. ID | $P$ (day) | $\langle I \rangle$ (mag) | $\langle V \rangle$ (mag) | R.A. | Decl. | $d$ (kpc)[a,b] | Age (Myr) rot.[c] | Age (Myr) no-rot.[d] |
|---|---|---|---|---|---|---|---|---|---|
| F | OGLE-SMC-CEP-4956 | | | | | | | | |
| | M1 | 1.1162345 | 17.372 | 17.930 | $03^h23^m24\overset{s}{.}90$ | $-74°58'07\overset{''}{.}3$ | 71.53 ± 2.00 | 567 | 283 ± 59 |
| | OGLE-SMC-CEP-4953 | | | | | | | | |
| | M4 | 21.3856352 | 12.965 | 13.824 | $02^h20^m49\overset{s}{.}46$ | $-73°05'08\overset{''}{.}3$ | 53.28 ± 1.49 | 48 | 27 ± 6 |
| | OGLE-SMC-CEP-4952[e] | | | | | | | | |
| | M7 | 1.6414839 | 16.901 | 17.535 | $02^h04^m09\overset{s}{.}38$ | $-77°04'38\overset{''}{.}4$ | 69.99 ± 1.97 | 410 | 209 ± 44 |
| | OGLE-SMC-CEP-4987[f] | | | | | | | | |
| | M10 | 2.9284749 | 15.738 | 16.458 | $03^h31^m34\overset{s}{.}40$ | $-70°59'38\overset{''}{.}2$ | 56.45 ± 1.56 | 252 | 132 ± 28 |
| | OGLE-SMC-CEP-4986[g] | | | | | | | | |
| | M11 | 16.4454990 | 13.480 | 14.378 | $02^h02^m59\overset{s}{.}72$ | $-74°03'24\overset{''}{.}7$ | 54.87 ± 1.53 | 59 | 34 ± 8 |
| 1O | OGLE-SMC-CEP-4955 | | | | | | | | |
| | M5 | 2.0308924 | 15.675 | 16.281 | $02^h42^m28\overset{s}{.}88$ | $-74°43'17\overset{''}{.}6$ | 59.58 ± 1.64 | 297 | 120 ± 20 |
| | OGLE-LMC-CEP-3377 | | | | | | | | |
| | M6 | 3.2144344 | 14.629 | 15.291 | $04^h04^m28\overset{s}{.}88$ | $-75°04'47\overset{''}{.}1$ | 48.38 ± 1.34 | 191 | 74 ± 13 |
| | OGLE-LMC-CEP-3380 | | | | | | | | |
| | M12 | 1.0178714 | 16.485 | 17.101 | $04^h35^m32\overset{s}{.}89$ | $-74°33'46\overset{''}{.}7$ | 53.62 ± 1.48 | 576 | 252 ± 41 |
| | OGLE-LMC-CEP-3381[h] | | | | | | | | |
| | M13 | 0.5188341 | 17.230 | 17.677 | $04^h37^m03\overset{s}{.}69$ | $-74°58'25\overset{''}{.}3$ | 53.84 ± 1.49 | 1101 | 519 ± 84 |
| 1O2O | OGLE-SMC-CEP-4951[h] | | | | | | | | |
| | M9 | 0.7170500 | 16.769 | 17.222 | $02^h02^m33\overset{s}{.}88$ | $-75°30'48\overset{''}{.}0$ | 54.06 ± 1.49 | 807 | 367 ± 60 |

**Notes.** All Cepheids except M1 and M7 form a continuous-like connection between the Magellanic Clouds.
[a] The distance uncertainty does not include the mean LMC distance uncertainty from Pietrzyński et al. (2019) $d_{\rm LMC} = 49.59 \pm 0.09$ (statistical) $\pm 0.54$ (systematic) kpc.
[b] For comparison of distance estimates using different techniques, see Table 4.
[c] This age value was estimated using the period–age relation for average instability strip crossing and including average initial rotation from Anderson et al. (2016).
[d] This age determination was estimated using the period–age relation from Bono et al. (2005). For other estimates see Table 3.
[e] This Cepheid was reclassified from first-overtone to fundamental-mode pulsator.
[f] This Cepheid was added to the sample by Soszyński et al. (2017).
[g] $V$-band magnitude for this Cepheid was calculated using ASAS-SN Sky Patrol (Schappee et al. 2014; Kochanek et al. 2017).
[h] Ages of short-period Cepheids may not be calculated properly (see details in Section 4.3).

(white circles), anomalous (red circles), and type II (green circles) Cepheids compared to the distribution of young stars from Skowron et al. (2014), as well as neutral hydrogen density contours from the Galactic All Sky H I Survey (McClure-Griffiths et al. 2009; Kalberla et al. 2010; Kalberla & Haud 2015). Larger circles distinguish the selected Bridge sample, while smaller circles show other Magellanic System Cepheids. Note that there is only one T2C in the highlighted area. Labels M1–M13 mark the CC sample from Paper I, as well as new CCs that we added to the final Bridge sample. Note that three of these objects were reclassified as ACs.

### 4.2. Two- and Three-dimensional Analysis

The on-sky locations of CCs in the MBR are presented using large white circles in Figure 3. Their locations match well with the H I density contours. Only two Cepheids, namely, M7 and M10, lie slightly offset from the peak H I density, though still well within contours showing the densest regions. Actually, the MBR CCs are forming an on-sky connection between the Magellanic Clouds following young stars' distribution (Skowron et al. 2014). Based on the on-sky locations, we conclude that all of our CCs in the Bridge match results from Paper I, where we stated that the CCs add to the overall distribution of the young population. For comparison we also show in Figure 3 ACs, which are marked with large red circles. ACs are definitely more spread out and do not follow the young stars' distribution, as was also already shown by other studies (Fiorentino & Monelli 2012; Iwanek et al. 2018).

Figure 4 shows three-dimensional distribution of CCs in the Magellanic System. Four out of five CCs that we listed in Paper I as constituting a genuine connection between the Magellanic Clouds, specifically M4, M5, M6, and M9, have not been reclassified, and their locations are the same as we presented therein. One out of these five, M3, was reclassified as AC. The four CCs that were lately added to the sample, M10–M13, add to the bridge-like structure. However, M12 and M13 may plausibly not belong to the genuine Bridge population, as they seem to be the LMC outliers located in the extended LMC structure. Similarly, M9 and M11 are located very close to the SMC Wing and thus may also be the Wing stars. On the other hand, the four LMC/SMC outliers may also add to the main MBR sample. Taking that into account, we report here that 8 out of 10 CCs in our updated sample contribute to a bridge-like connection between the Magellanic Clouds.

The farthest CCs in our sample are M1 and M7. M7 is one of the two CCs that are located slightly offset from the H I contours and the young population density distribution (see Figure 3). This suggests that M7 and M10 may have a different origin than CCs discussed in the previous paragraph. Yet, they may still constitute the genuine Bridge population. To test that, other parameters than discussed in this paper need to be taken into account (i.e., chemical composition). However, these Cepheids could also be members of the Counter Bridge, predicted by the numerical

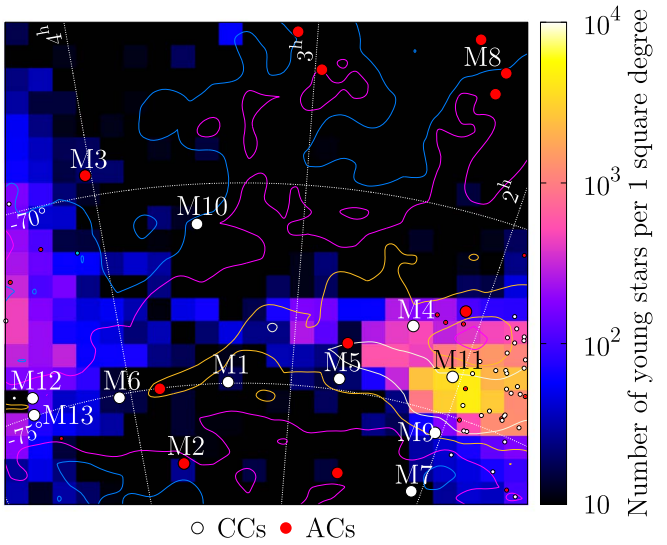


**Figure 3.** On-sky locations of the central Bridge Cepheid sample as compared to the color-coded young stars' column density from Skowron et al. (2014) and neutral hydrogen density contours from the Galactic All Sky H I Survey (McClure-Griffiths et al. 2009; Kalberla et al. 2010; Kalberla & Haud 2015). Different types of Cepheids are marked with different colors. The selected Bridge sample is featured with larger circles, while smaller circles show LMC and SMC Cepheids. Labels M1–M9 mark the classical Cepheid sample from Paper I, and M10–M13 are new classical Cepheids that we added to the final MBR sample. M2, M3, and M8 were lately reclassified as anomalous Cepheids. The H I is integrated over the velocity range 80 km $s^{-1} < v < 400$ km $s^{-1}$. Contours are on the levels $(1, 2, 4, 8) \cdot 10^{20}$ $cm^{-2}$. The color-coded value of each box is a logarithm of the number of young stars per square degree area (each pixel is ≈0.335 $deg^2$). The map is represented in a Hammer equal-area projection centered at $\alpha_{cen} = 3^h18^m$, $\delta_{cen} = -70°$. This plot is an updated version of Figure 18 from Paper I.

model by Diaz & Bekki (2012). This structure was already discussed in Paper I in terms of the three-dimensional distribution of our previous sample, where we classified two CCs as plausible members of the Counter Bridge. Both were reclassified—M8 as AC and M7 as first-overtone CC—from fundamental-mode CC to first-overtone pulsator (Section 6). With the updated sample we do not have as evident candidates as before, though M1 and M7 are located near the borders of the Counter Bridge (see Figure 17 in Ripepi et al. 2017).

Our Bridge sample is not as spread out in terms of distances as the sample presented in Paper I. All of the CCs are located in between the Magellanic Clouds, being farther than the closest LMC Cepheid and closer than the farthest SMC Cepheid. On the other hand, not all of the Bridge CCs form an evident, bridge-like connection. Some of these stars may also be ejected from the LMC and/or SMC instead of forming the genuine Bridge. Indeed, we do see some individual objects spread over in different directions near these galaxies. The origin of our Bridge CCs will not be fully understood until further analyses are carried out taking into account different parameters than the ones we present in this paper. Of special importance are spectroscopic observations that could lead to a definite classification of these objects.

### 4.3. Ages

Ages of our CCs were estimated using the period–age relation from Anderson et al. (2016) and Bono et al. (2005). The main difference between these two is that the former includes average rotation, while the latter does not include stellar rotation at all. As we have already discussed in Paper I (see Section 6 therein), the Bridge has metallicity similar to or smaller than the SMC (Lehner et al. 2008; Misawa et al. 2009). Neither Anderson et al. (2016) nor Bono et al. (2005) provide any relation for metallicity smaller than the SMC; thus, we applied to our Bridge sample the relation for the SMC metallicity. Calculated values are presented in Tables 2 and 3.

Table 3 presents the age estimates based on the period–age relation from Anderson et al. (2016) and Bono et al. (2005), as well as values obtained using the period–age–color relation (we used relations for the SMC metallicity). The relations from Anderson et al. (2016) were derived from theoretical models including rotation. Age values that they provide are approximately twice as large as values obtained using Bono et al. (2005) relations. This should not be surprising, as rotation induces mixing in stellar interiors, which leads to refreshing the core hydrogen supplies. Thus, a rotating star can be burning hydrogen for a longer time than a nonrotating one. As a result, the star can remain on the main sequence for a longer period of time and then cross the instability strip and become a Cepheid at an older age. Results from both relations from Bono et al. (2005) match well within the error bars.

Including rotation, 5 out of 10 CCs in our Bridge sample are younger than 300 Myr. This is in agreement with an assumption that these objects were formed in situ after the last encounter of the Magellanic Clouds (e.g., Gardiner et al. 1994; Gardiner & Noguchi 1996; Růžička et al. 2010; Besla et al. 2012; Diaz & Bekki 2012; Zivick et al. 2019). All of these five CCs are constituting a connection between the LMC and SMC, as we have described in the previous section. These are the CCs indexed M4, M5, M6, M10, and M11.

Two CCs in our sample are younger than 60 Myr. These are M4 (48 Myr) and M11 (59 Myr), which are located close to the SMC. Both may be stars ejected from this galaxy. The two oldest CCs in our sample, M9 and M13, are also the shortest-period pulsators. The age determination is 807 Myr for M9 and 1101 Myr for M13. These values seem rather large and could be incorrect owing to the fact that models do not predict ages of objects with such short periods. That is why we treat these estimates as rather rough.

### 4.4. Proper Motions

We used *Gaia* DR2 (Gaia Collaboration et al. 2018) to analyze PMs of our Bridge CCs. Following Kallivayalil et al. (2013) and Zivick et al. (2018, 2019), we use here $\mu_N = \mu_\delta$ and $\mu_W = -\mu_\alpha \cos\delta$, where $\alpha$, $\delta$ are R.A., decl., respectively. We compare our results to the LMC and SMC PMs (Kallivayalil et al. 2013; Zivick et al. 2018) in Figures 5 and 6. CC PMs follow the general on-sky movement of the Magellanic System. PMs of M12 and M13 are relatively very similar to the LMC PM, while PMs of M9 and M11 are relatively very similar to the SMC PM. This supports our conclusions from the previous subsection that these Cepheids are probably LMC and SMC outliers. All of the other Bridge CC PM values fall in between those of LMC and SMC. This is what we would expect for a Bridge population (see Figure 3 in Zivick et al. 2019).

Figure 6 shows PMs of Bridge CCs, as well as the LMC and SMC PMs, plotted as vectors on the sky. CC PMs as related to the LMC or SMC are rather low and comparable to the Clouds' relative PM. In the LMC-related frame all CCs are moving away from this galaxy. For the SMC-related PMs the situation

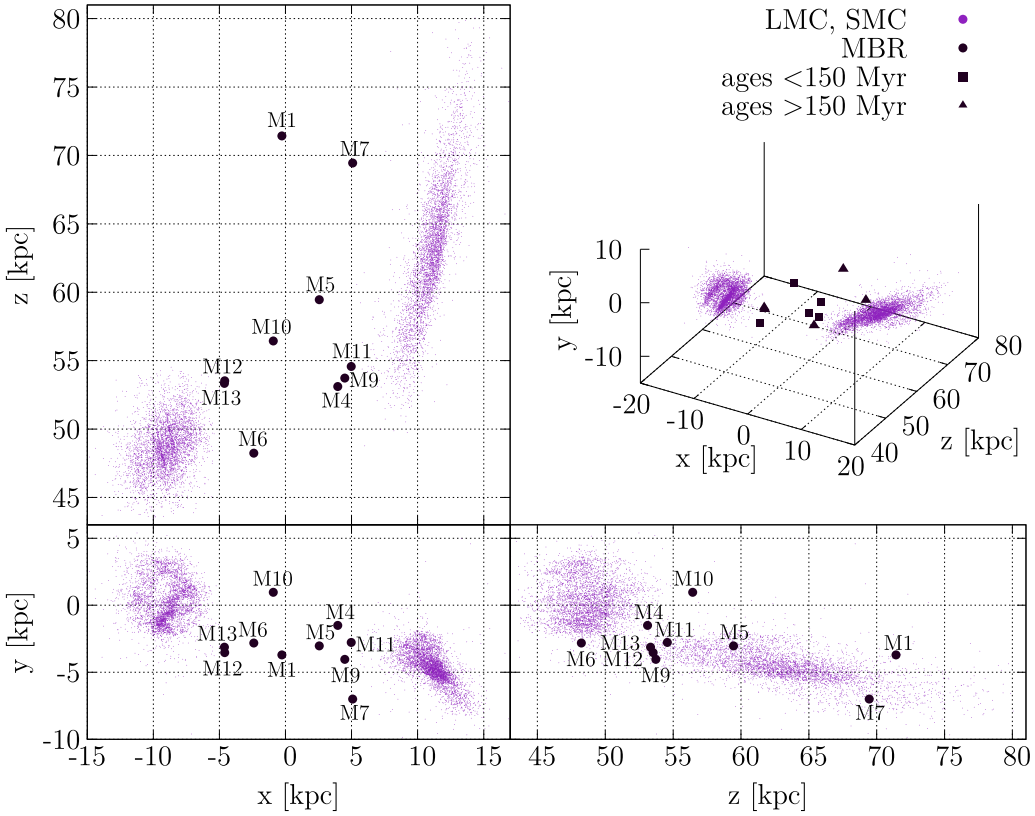


**Figure 4.** Three-dimensional distribution of classical Cepheids in the Magellanic System, with the MBR sample marked with large circles. Labels show local IDs of these objects (see Table 2). The map is represented in Cartesian coordinates with the observer located at (0, 0, 0). Ages were calculated using relations from Bono et al. (2005).

**Table 3**
Magellanic Bridge Classical Cepheids: Ages

| Mode | Loc. ID | $P$ (day)[a] | $\mathrm{Age_{rot}}$(Myr)[b] | $\mathrm{Age_{PA}}$(Myr)[c] | $\mathrm{Age_{PAC}}$(Myr)[d] |
|---|---|---|---|---|---|
| F | M1 | 1.1 | 567 | 283 ± 59 | 271 ± 63 |
| | M4 | 21.4 | 48 | 27 ± 6 | 27 ± 8 |
| | M7 | 1.6 | 410 | 209 ± 44 | 207 ± 50 |
| | M10 | 2.9 | 252 | 132 ± 28 | 110 ± 26 |
| | M11 | 16.4 | 59 | 34 ± 8 | 35 ± 10 |
| 1O | M5 | 2.0 | 297 | 120 ± 20 | 123 ± 22 |
| | M6 | 3.2 | 191 | 74 ± 13 | 79 ± 15 |
| | M12 | 1.0 | 576 | 252 ± 41 | 279 ± 50 |
| | M13[e] | 0.5 | 1101 | 519 ± 84 | 475 ± 77 |
| 1O2O | M9[e] | 0.7 | 807 | 367 ± 60 | 329 ± 54 |

**Notes.**
[a] Find a more precise period determination in Table 2.
[b] Calculated using the period–age relation from Anderson et al. (2016) that includes average stellar rotation on an average instability strip crossing.
[c] Calculated using the period–age relation from Bono et al. (2005).
[d] Calculated using the period–age–color relation from Bono et al. (2005).
[e] Ages of short-period Cepheids may not be calculated properly (see details in Section 4.3).

is similar. This means that the Bridge CCs are moving away from both Clouds.

### 4.5. Different Distance Estimates

The Cepheid PL relation has an intrinsic dispersion caused by a finite width of the instability strip (e.g., Anderson et al. 2016) and/or depth effects (e.g., Inno et al. 2013; Scowcroft et al. 2016; Paper I). This implies that the PL relations are more useful for estimating the sample's mean distance than individual distances of each Cepheid. The natural spread of PL relations is significantly smaller in the infrared (e.g., Storm et al. 2011; Ngeow et al. 2015; Scowcroft et al. 2016; Gallenne et al. 2017; Madore et al. 2017). However, one can obtain useful PL relations in the optical regime with Wesenheit magnitude that combines two passbands and includes a color term (Udalski et al. 1999; Fouqué et al. 2007; Soszyński et al. 2008; Ngeow 2012; Lemasle et al. 2013; Anderson et al. 2016; Paper I). Ngeow (2012) showed

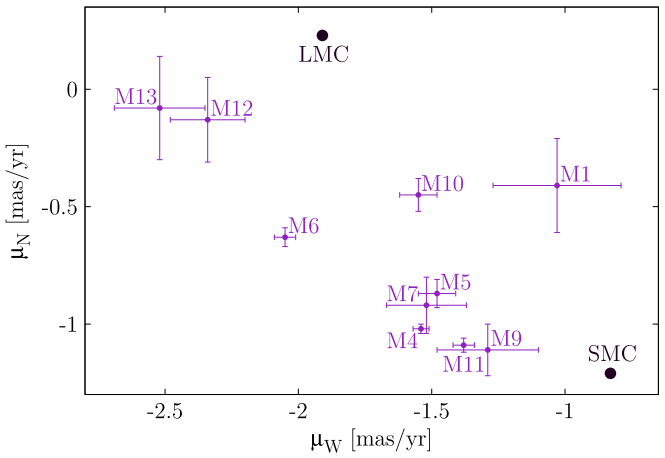


**Figure 5.** PMs of Bridge CCs as compared to the PM of the LMC (Kallivayalil et al. 2013) and SMC (Zivick et al. 2018). All 10 CCs from our sample are marked with their local IDs.

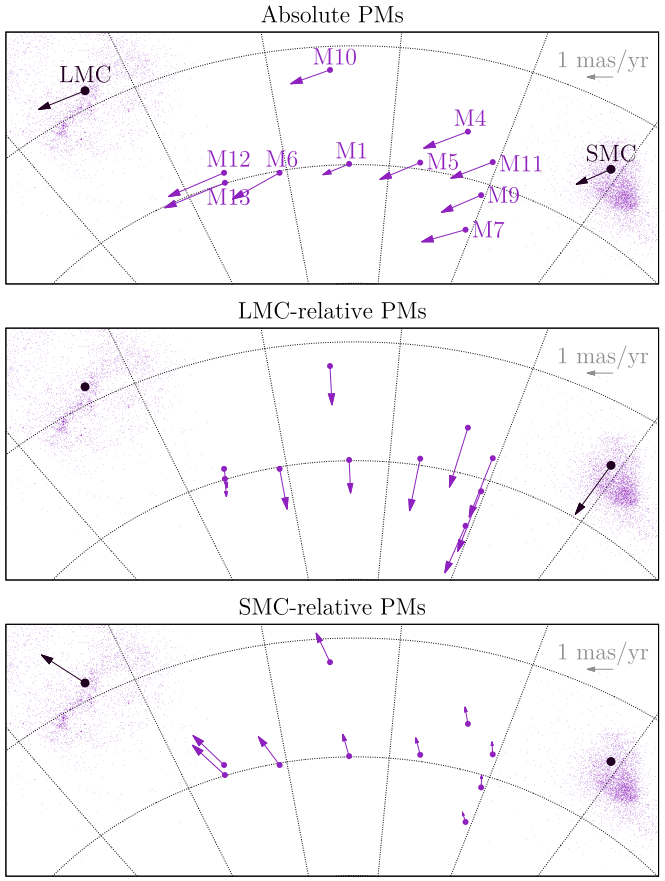


**Figure 6.** PMs of Bridge CCs, as well as LMC (Kallivayalil et al. 2013) and SMC (Zivick et al. 2018), shown as vectors on the sky. The top panel presents absolute PMs, while the middle and bottom panels present the LMC- and SMC-related frame, respectively. We adopted the LMC center of van der Marel & Kallivayalil (2014) and the SMC center of Stanimirović et al. (2004).

that the period–Wesenheit relations can be used to determine individual distances of Galactic Cepheids. Here we have also tried other techniques to calculate individual distances of our MBR CC sample. The results are shown in Table 4 and Figure 7 and discussed in this section.

As described in Section 3.1, our basic method of calculating distances is the same as we used in Paper I. It relies on the

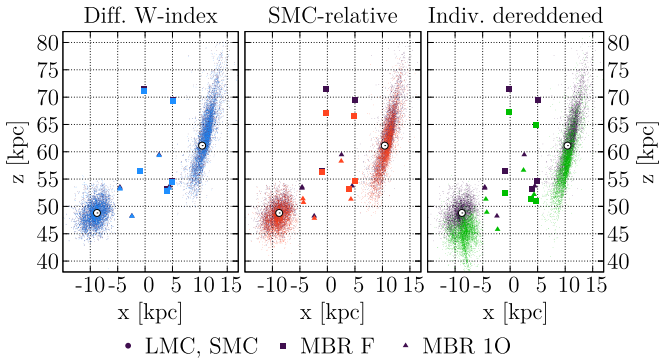


**Figure 7.** Three-dimensional distribution of CCs in the Magellanic System in Cartesian *x*-*z* plane projection. The distribution obtained using our basic distance estimates (as described in Section 3.1) is marked with black in every panel. Overplotted are, for comparison, different distributions marked with colored circles (see text for details). The Bridge CC sample is highlighted with larger symbols. In all of the panels white circles mark LMC (Pietrzyński et al. 2019; van der Marel & Kallivayalil 2014) and SMC (Graczyk et al. 2014; Stanimirović et al. 2004) centers.

Wesenheit PL relation for the LMC and an assumption that the fit corresponds to the mean LMC distance (Pietrzyński et al. 2019). We called this distance estimate $d_{\rm LMC}$, as it is related to the LMC, and show it in the fourth column in Table 4 (as well as in Table 2). The resulting uncertainty does not include uncertainty from Pietrzyński et al. (2019), as it would only lead to a systematic error, which would be the same for our entire sample. In order to test how the adopted reddening law influences individual distances, we also calculated distances the same way but with a different color term coefficient in the Wesenheit index. Instead of 1.55 we used 1.44 (see Equation (6) in Paper I and Udalski 2003). The results are shown as $d_{\rm LMC,W44}$ (fifth column in Table 4) and match very well our basic distances, although the former are slightly smaller. For comparison, see also the left panel of Figure 7, where the three-dimensional distribution obtained with basic distances is marked with black circles, while with that a different reddening law is marked with blue circles and is overplotted on the former. This also means that the adopted reddening law does not have much impact on the Bridge Cepheids' distances. This is in agreement with the fact that the reddening toward the MBR is low (Schlegel et al. 1998; Wagner-Kaiser & Sarajedini 2017, Skowron et al. 2019, in preparation).

We also calculated distances in relation to the SMC ($d_{\rm SMC}$; sixth column in Table 4). We used the same technique as in our basic approach but adopted the SMC fit and the SMC mean distance as a reference (Graczyk et al. 2014). The resulting distances are smaller than our basic values, and the difference is up to 5 kpc in some cases, even though the geometry of the entire LMC and SMC samples does not differ much using both approaches. This is shown in the middle panel of Figure 7, where we overplotted the three-dimensional distribution relative to the SMC (red) on that relative to the LMC (black). This incoherence may be caused by the fact that our SMC sample reveals a slightly larger mean distance when using our basic method than that from Graczyk et al. (2014). Thus, when we changed the reference point to the SMC, the entire sample moved slightly closer.

Having magnitudes in both OGLE passbands, *I* and *V*, we could also deredden our data. This is the same approach as used by Haschke et al. (2012a, 2012b). First, we calculated absolute magnitudes using PL relations from Sandage et al. (2004, 2009) that were derived for the LMC and SMC data

**Table 4**
Magellanic Bridge Classical Cepheids: Distances

| Mode | Loc. ID | $P$ (day)[a] | $d_{\rm LMC}$ (kpc)[b] | $d_{\rm LMC,\ W44}$ (kpc)[b] | $d_{\rm SMC}$ (kpc)[c] | $d_{\rm red}$ (kpc) |
|---|---|---|---|---|---|---|
| F | M1 | 1.1 | 71.53 ± 2.00 | 71.17 ± 1.89 | 67.22 ± 1.86 | 67.37 ± 10.83 |
| | M4 | 21.4 | 53.28 ± 1.49 | 53.00 ± 1.41 | 53.43 ± 1.50 | 51.53 ± 7.46 |
| | M7 | 1.6 | 69.99 ± 1.97 | 69.87 ± 1.87 | 66.98 ± 1.85 | 65.40 ± 10.25 |
| | M10 | 2.9 | 56.45 ± 1.56 | 56.45 ± 1.49 | 56.29 ± 1.56 | 52.39 ± 7.73 |
| | M11 | 16.4 | 54.87 ± 1.53 | 54.80 ± 1.46 | 55.30 ± 1.55 | 51.24 ± 7.36 |
| 1O | M5 | 2.0 | 59.58 ± 1.64 | 59.42 ± 1.56 | 58.39 ± 1.61 | 56.74 ± 8.33 |
| | M6 | 3.2 | 48.38 ± 1.34 | 48.31 ± 1.27 | 47.95 ± 1.33 | 45.91 ± 6.40 |
| | M12 | 1.0 | 53.62 ± 1.48 | 53.61 ± 1.40 | 51.66 ± 1.43 | 49.18 ± 7.51 |
| | M13 | 0.5 | 53.84 ± 1.49 | 53.47 ± 1.40 | 51.01 ± 1.41 | 51.62 ± 8.21 |
| 1O2O | M9 | 0.7 | 54.06 ± 1.49 | 53.66 ± 1.41 | 51.63 ± 1.42 | 52.50 ± 8.14 |

**Notes.**
[a] Find a more precise period determination in Table 2.
[b] The distance uncertainty does not include the mean LMC distance uncertainty from Pietrzyński et al. (2019) $d_{\rm LMC} = 49.59 \pm 0.09$ (statistical) $\pm 0.54$ (systematic) kpc.
[c] The distance uncertainty does not include the mean LMC distance uncertainty from Graczyk et al. (2014) $d_{\rm SMC} = 62.1 \pm 1.9$ kpc.

**Table 5**
Magellanic Bridge Classical Cepheids: Absolute Magnitudes

| Loc. ID | $M_I$ (mag)[a] | $M_{I,2}$ (mag)[b] | $M_V$ (mag)[a] | $M_{V,2}$ (mag)[b] | $E(V-I)$ (mag) | $E(V-I)_2$ (mag) |
|---|---|---|---|---|---|---|
| M1 | −1.984 ± 0.028 | −1.742 ± 0.184 | −1.524 ± 0.036 | −1.175 ± 0.209 | 0.098 ± 0.053 | −0.009 ± 0.280 |
| M4 | −5.654 ± 0.054 | −5.504 ± 0.057 | −4.842 ± 0.070 | −4.644 ± 0.063 | 0.048 ± 0.093 | −0.001 ± 0.089 |
| M7 | −2.463 ± 0.029 | −2.233 ± 0.159 | −1.957 ± 0.037 | −1.628 ± 0.181 | 0.128 ± 0.054 | 0.029 ± 0.242 |
| M10 | −3.183 ± 0.032 | −2.971 ± 0.123 | −2.608 ± 0.041 | −2.308 ± 0.139 | 0.145 ± 0.059 | 0.057 ± 0.188 |
| M11 | −5.327 ± 0.051 | −5.170 ± 0.052 | −4.547 ± 0.065 | −4.336 ± 0.058 | 0.118 ± 0.087 | 0.072 ± 0.082 |
| M5 | −3.140 ± 0.032 | −2.928 ± 0.125 | −2.569 ± 0.041 | −2.268 ± 0.141 | 0.035 ± 0.059 | −0.053 ± 0.191 |
| M6 | −3.723 ± 0.036 | −3.525 ± 0.097 | −3.096 ± 0.046 | −2.819 ± 0.109 | 0.035 ± 0.065 | −0.044 ± 0.149 |
| M12 | −2.264 ± 0.028 | −2.029 ± 0.170 | −1.777 ± 0.036 | −1.440 ± 0.192 | 0.129 ± 0.054 | 0.027 ± 0.258 |
| M13 | −1.410 ± 0.028 | −1.153 ± 0.215 | −1.004 ± 0.036 | −0.633 ± 0.243 | 0.042 ± 0.054 | −0.074 ± 0.325 |
| M9 | −1.820 ± 0.028 | −1.574 ± 0.193 | −1.375 ± 0.036 | −1.020 ± 0.219 | 0.009 ± 0.053 | −0.101 ± 0.293 |

**Notes.** For first-overtone pulsators we used fundamentalized periods.
[a] Calculated using relations from Sandage et al. (2004, 2009).
[b] Calculated using relations from Gieren et al. (2018).

separately. We applied the SMC relations to the MBR sample, as the Bridge metallicity is close to or slightly lower than the SMC metallicity (e.g., Lehner et al. 2008; Misawa et al. 2009; Carrera et al. 2017; Wagner-Kaiser & Sarajedini 2017). We used relations not including the PL break at $\log P = 1$, as the samples used to derive these relations only consisted of Cepheids with $\log P > 0.4$. Half of our Bridge sample are CCs with shorter periods; thus, we extrapolate these PL relations. Moreover, it was shown that the break at $\log P = 1$ is not significant, at least for the SMC (Bhardwaj et al. 2016).

The PL relations that we used for the LMC (Sandage et al. 2004) are

$$M_I = (-2.949 \pm 0.020)\log P - (1.936 \pm 0.015) \quad (6)$$

$$M_V = (-2.701 \pm 0.035)\log P - (1.491 \pm 0.027). \quad (7)$$

Those for the SMC (Sandage et al. 2009) are

$$M_I = (-2.862 \pm 0.028)\log P - (1.847 \pm 0.022) \quad (8)$$

$$M_V = (-2.588 \pm 0.045)\log P - (1.400 \pm 0.035). \quad (9)$$

These relations were derived only for the fundamental-mode pulsators. For the first-overtone CCs in our sample we fundamentalized the periods using the relation between periods from Alcock et al. (1995) (as in Groenewegen & Oudmaijer 2000):

$$P_{\rm 1O}/P_{\rm F} = 0.733 - 0.034\log P_{\rm F},\ 0.1 < \log P_{\rm F} \leqslant 0.7. \quad (10)$$

We have simplified the above equation and used the following form:

$$P_{\rm F} = P_{\rm 1O}/(0.728 - 0.034\log P_{\rm 1O}). \quad (11)$$

This relation does not account for metallicity dependence of the ratio of the fundamental-mode and the first-overtone periods (Szilądi et al. 2007, 2018). We used data for double-mode Cepheids in the LMC and SMC (Soszyński et al. 2015b) to verify the possible error that could arise from this simplification. We found that the median difference between the real fundamental mode of the Cepheid and the one calculated from its first-overtone period is 0.2% in the case of the LMC and 1.3% in the case of the SMC. This translates to differences in distance of order ∼1%, which do not influence this analysis.

It is noteworthy that relations for the LMC were derived using a significantly different mean distance modulus to this

**Table 6**
Magellanic Bridge Classical Cepheids: Reddening Parameters

| Loc. ID | $A_I$ (mag)[a] | $A_{I,W44}$ (mag)[b] | $A_{I,t}$ (mag)[c] | $A_V$ (mag)[a] | $A_{V,W44}$ (mag)[b] | $A_{V,t}$ (mag)[c] |
|---|---|---|---|---|---|---|
| M1 | 0.083 ± 0.070 | 0.094 ± 0.067 | 0.248 ± 0.134 | 0.181 ± 0.073 | 0.192 ± 0.071 | 0.150 ± 0.081 |
| M4 | −0.014 ± 0.084 | −0.002 ± 0.082 | 0.121 ± 0.234 | 0.034 ± 0.095 | 0.045 ± 0.093 | 0.073 ± 0.142 |
| M7 | 0.139 ± 0.070 | 0.143 ± 0.070 | 0.325 ± 0.137 | 0.267 ± 0.074 | 0.271 ± 0.072 | 0.196 ± 0.083 |
| M10 | 0.162 ± 0.071 | 0.162 ± 0.069 | 0.368 ± 0.150 | 0.307 ± 0.076 | 0.307 ± 0.073 | 0.223 ± 0.091 |
| M11 | 0.111 ± 0.082 | 0.113 ± 0.080 | 0.319 ± 0.221 | 0.236 ± 0.091 | 0.239 ± 0.090 | 0.193 ± 0.134 |
| M5 | −0.061 ± 0.071 | −0.055 ± 0.068 | 0.089 ± 0.149 | −0.025 ± 0.075 | −0.019 ± 0.073 | 0.054 ± 0.090 |
| M6 | −0.071 ± 0.073 | −0.069 ± 0.070 | 0.090 ± 0.164 | −0.036 ± 0.078 | −0.033 ± 0.076 | 0.054 ± 0.099 |
| M12 | 0.102 ± 0.069 | 0.103 ± 0.067 | 0.327 ± 0.135 | 0.231 ± 0.073 | 0.232 ± 0.070 | 0.198 ± 0.082 |
| M13 | −0.016 ± 0.069 | −0.001 ± 0.067 | 0.106 ± 0.135 | 0.026 ± 0.073 | 0.041 ± 0.070 | 0.064 ± 0.082 |
| M9 | −0.076 ± 0.069 | −0.059 ± 0.066 | 0.022 ± 0.134 | −0.067 ± 0.073 | −0.051 ± 0.070 | 0.013 ± 0.081 |

**Notes.** All parameters based on absolute magnitudes were calculated using relations from Sandage et al. (2004, 2009) (see Table 5). This is only an estimate, and we discourage using values presented here in scientific research, as many obtained parameters are nonphysical (values under zero).
[a] Total reddening obtained using basic method distances.
[b] Total reddening obtained using distances calculated assuming different reddening law (different color term coefficient in Wesenheit index as described in Section 4.5).
[c] Theoretical total reddening calculated without assuming any distance to each Cepheid. Here we used Schlegel et al. (1998) reddening laws (see Equation (12)).

galaxy. Sandage et al. (2004) based their calculations on the value from Tammann et al. (2003), which is $\mu_{\rm LMC} = 18.54$ mag. In our basic approach we use $\mu_{\rm LMC} = 18.477$ mag (Pietrzyński et al. 2019). For the SMC the difference is not that significant. Sandage et al. (2009) use $\mu_{\rm SMC} = 18.93$ mag (Tammann et al. 2008), while Graczyk et al. (2014) obtain $\mu_{\rm SMC} = 18.965$ mag.

Following the Haschke et al. (2012a, 2012b) approach, in the next step we calculated color excess for each Cepheid $E(V-I) = (m_V - m_I) - (M_V - M_I)$, where $m_{V,I}$ are observed magnitudes and $M_{V,I}$ are absolute magnitudes in the appropriate filter. We noticed a mistake in Haschke et al. (2012a), Equations (6) and (7), that appears when trying to subtract one from another, and $A(V) - A(I)$ does not result in $E(V-I)$. We thus calculated these relations based on original Schlegel et al. (1998) coefficients to obtain total extinction in each passband:

$$A_V = 3.24(E(V-I)/1.278) \quad (12)$$

$$A_I = 1.96(E(V-I)/1.278). \quad (13)$$

Note that there is 1.278 in the denominator instead of 1.4 as in Haschke et al. (2012a). Calculated reddening parameters are shown in Table 6 and discussed in the following section, as here we concentrate on distances. To calculate distance moduli, we used the $I$-band magnitudes, as these values are usually more accurate than $V$-band ones. The distance modulus is simply

$$\mu = m_I - M_I - A_I, \quad (14)$$

and distance is

$$d = 10^{(5+\mu)/5}. \quad (15)$$

Results are presented in the last column of Table 4 and in the right panel of Figure 7. The individual dereddening technique resulted in significantly lower distances for every CC in the Bridge sample than previously discussed methods. Moreover, this technique has changed the entire geometry of the LMC and SMC samples, as is clearly visible in Figure 7. Our basic method relying on fitting the PL relations to the observational data is very robust, which was proven by many different surveys (e.g., Haschke et al. 2012a, 2012b; Moretti et al. 2014; Paper I; Inno et al. 2016; Ripepi et al. 2017). Thus, we do not think that the individual dereddening technique is suitable to properly determine distances to Magellanic System Cepheids and especially to infer any conclusions about structure and geometry.

### 4.6. Reddening Parameters

Table 5 shows local IDs and absolute magnitudes in $I$ and $V$ bands, as well as color excesses of our Bridge CCs. For each passband we present two values for each parameter calculated using different PL relations (Sandage et al. 2004, 2009; Gieren et al. 2018). As expected, the longer the period, the younger the Cepheid, and thus more luminous. Relations from Sandage et al. (2004, 2009) have significantly different zero-points than those of Gieren et al. (2018), and this results in CCs being less luminous in the latter case. Relations from Gieren et al. (2018) also have larger uncertainties, and this is reflected in Table 5. On the other hand, slopes are very consistent.

Color excesses, $E(V-I)$, in general have quite low values, consistent with the fact that there is low extinction toward the Bridge area (Schlegel et al. 1998; Wagner-Kaiser & Sarajedini 2017, Skowron et al. 2019, in preparation). $E(V-I)$ calculated using relations from Gieren et al. (2018) in many cases have values that are physical only within the error bars; thus, we use absolute magnitudes based on Sandage et al. (2004, 2009) in further analysis. The discrepancy is probably due to a difference in zero-points between these relations. However, we also note that relations from Gieren et al. (2018) were derived for CCs with periods 4 days $< P <$ 69 days, and only 3 out of 10 of our CCs fall into this range.

Values obtained for color excesses of each CC are very well consistent with the mean value of this parameter found toward the Bridge by Wagner-Kaiser & Sarajedini (2017), who studied RRab-type stars in that area. Their median is $E(V-I) = 0.101 \pm 0.007$ mag.

Table 6 presents reddening parameters for our Bridge CCs calculated using absolute magnitudes based on PL relations from Sandage et al. (2004, 2009). $A_{I,V}$ are total extinctions

**Table 7**
Magellanic Bridge Anomalous Cepheids: Basic Parameters

| Mode | OCVS ID | Loc. ID[a] | $P$ (day) | $\langle I\rangle$ (mag) | $\langle V\rangle$ (mag) | R.A. | Decl. | $d$ (kpc)[b] |
|---|---|---|---|---|---|---|---|---|
| F | OGLE-LMC-ACEP-084 | ⋯ | 2.0506071 | 17.033 | 17.859 | $03^h49^m00\overset{s}{.}53$ | $-75°00'49\overset{''}{.}1$ | 51.38 ± 1.46 |
| | OGLE-LMC-ACEP-085 | ⋯ | 0.9156319 | 17.358 | 17.974 | $03^h59^m33\overset{s}{.}43$ | $-63°16'40\overset{''}{.}5$ | 43.01 ± 1.19 |
| | OGLE-SMC-ACEP-100 | ⋯ | 1.6414839 | 17.405 | 17.908 | $02^h05^m36\overset{s}{.}66$ | $-72°24'19\overset{''}{.}9$ | 46.05 ± 1.28 |
| | OGLE-SMC-ACEP-104 | ⋯ | 0.8780260 | 17.197 | 17.654 | $02^h14^m51\overset{s}{.}37$ | $-66°59'30\overset{''}{.}4$ | 43.64 ± 1.21 |
| | OGLE-SMC-ACEP-105 | ⋯ | 0.7559469 | 18.218 | 18.840 | $02^h30^m22\overset{s}{.}39$ | $-79°08'25\overset{''}{.}9$ | 56.81 ± 1.58 |
| | OGLE-SMC-ACEP-106 | ⋯ | 1.5007656 | 17.425 | 18.096 | $02^h37^m03\overset{s}{.}85$ | $-77°03'02\overset{''}{.}8$ | 57.14 ± 1.60 |
| | OGLE-SMC-ACEP-107 | ⋯ | 0.9317619 | 17.254 | 17.755 | $02^h41^m27\overset{s}{.}95$ | $-73°48'45\overset{''}{.}1$ | 44.97 ± 1.25 |
| | OGLE-SMC-ACEP-108 | ⋯ | 0.9147562 | 18.000 | 18.589 | $02^h58^m18\overset{s}{.}94$ | $-67°05'46\overset{''}{.}8$ | 58.90 ± 1.63 |
| | OGLE-SMC-ACEP-109 | ⋯ | 1.1701982 | 17.749 | 18.326 | $03^h04^m44\overset{s}{.}43$ | $-66°11'15\overset{''}{.}1$ | 61.23 ± 1.70 |
| | OGLE-LMC-ACEP-146[c,d] | M2 | 1.4300017 | 17.376 | 18.112 | $03^h43^m04\overset{s}{.}54$ | $-76°56'02\overset{''}{.}6$ | 51.83 ± 1.45 |
| | OGLE-GAL-ACEP-028[c,e] | M3 | 1.1589986 | 15.892 | 16.350 | $04^h01^m38\overset{s}{.}02$ | $-69°28'40\overset{''}{.}5$ | 28.18 ± 0.79 |
| 1O | OGLE-SMC-ACEP-102 | ⋯ | 0.9396136 | 17.347 | 17.904 | $02^h13^m39\overset{s}{.}52$ | $-66°25'17\overset{''}{.}0$ | 58.35 ± 1.67 |
| | OGLE-SMC-ACEP-122[f] | M8 | 0.8883309 | 17.302 | 17.738 | $02^h21^m28\overset{s}{.}45$ | $-65°45'22\overset{''}{.}4$ | 60.05 ± 1.72 |
| | OGLE-LMC-ACEP-147 | ⋯ | 0.7777591 | 16.537 | 16.961 | $04^h35^m35\overset{s}{.}29$ | $-81°06'21\overset{''}{.}0$ | 39.01 ± 1.13 |

**Notes.**
[a] Local IDs are provided only for ACs reclassified from CCs.
[b] The distance uncertainty does not include the mean LMC distance uncertainty from Pietrzyński et al. (2019) $d_{\rm LMC} = 49.59 \pm 0.09$ (statistical) $\pm 0.54$ (systematic) kpc.
[c] These objects were reclassified from fundamental-mode CCs.
[d] Former OGLE-SMC-CEP-4957.
[e] Former OGLE-LMC-CEP-3376. This Cepheid was reclassified as a Milky Way object owing to its proximity.
[f] This object was reclassified from first-overtone CC. Former OGLE-SMC-CEP-4954.

**Table 8**
PL Relations for ACs in the Magellanic System in the Wesenheit Magnitude

| $W_{I,V-I} = a \log P + b$ | | | | | | | |
|---|---|---|---|---|---|---|---|
| Galaxy | P. Mode | $a$ | $b$ (mag) | $\sigma$ (mag) | $\chi^2$/dof | $N_{\rm inc}$ | $N_{\rm rej}$ |
| LMC | F | −2.960 ± 0.044 | 16.599 ± 0.007 | 0.165 | 7.880 | 97 | 4 |
| | 1O | −3.297 ± 0.081 | 16.041 ± 0.017 | 0.144 | 6.260 | 39 | 1 |
| SMC | F | −2.725 ± 0.054 | 16.927 ± 0.009 | 0.178 | 9.228 | 74 | 1 |
| | 1O | −3.710 ± 0.094 | 16.539 ± 0.017 | 0.169 | 8.592 | 40 | 0 |

**Note.** F stands for fundamental mode, while 1O stands for first-overtone pulsators. $N_{\rm inc}$ is the number of objects included in the fit, while $N_{\rm rej}$ is the number of objects rejected during the $3\sigma$-clipping procedure.

obtained using our basic method distances, and $A_{(I,V),W44}$ are calculated using distances obtained with a slightly different reddening law—assuming a different color term coefficient in the Wesenheit index (as described in Section 4.5). Both values are very similar, showing again that the adopted reddening law does not influence our technique much. However, the total extinction is of a quite low value, close to zero, and has a rather low precision (uncertainties are twice the obtained values or even higher). In some cases, the obtained value is even less than zero. We want to emphasize here that these values are still physical, as they are consistent with zero or very low positive values within the error bars.

Similarly to Haschke et al. (2012a, 2012b), we also calculated extinction without using a priori distances but assuming a reddening law as described in Section 4.5 (see Equation (12)). Results are shown in Table 6 as $A_{(I,V),t}$. Values obtained for $I$ passband are significantly larger than resulting from previously described methods, however, surprisingly, they are consistent within the error bars. The $V$-band extinction matches quite well with values obtained using other techniques. On the other hand, the error bars for $A_{(I,V),t}$ are quite high.

## 5. Anomalous Cepheids

### 5.1. Final Sample and Basic Parameters

We used the recently published OGLE Collection of ACs in the Magellanic System (Soszyński et al. 2017) to construct our Bridge sample. Based on three-dimensional locations of these stars in comparison to the entire LMC and SMC samples, we decided to classify 10 ACs as Bridge candidates. Due to the latest updates and corrections applied to the OCVS (see Section 2.1), three Bridge CCs were reclassified as ACs. That enlarged our AC MBR sample to 13. Table 7 shows basic parameters of these objects: OCVS ID, local ID used in Paper I and this work (only for Cepheids reclassified from CCs to ACs), pulsation period $P$, mean magnitudes from both OGLE passbands ($I$ and $V$), R.A. and decl. (epoch J2000.0), and distance $d$.

To calculate individual distances of ACs, we used the same technique as for CCs (Section 3.1). We applied one exception to $3\sigma$ clipping. We did not exclude one anomalous Cepheid from our sample that was treated by our algorithm as an outlier, namely, OGLE-LMC-ACEP-147. This star is located in the

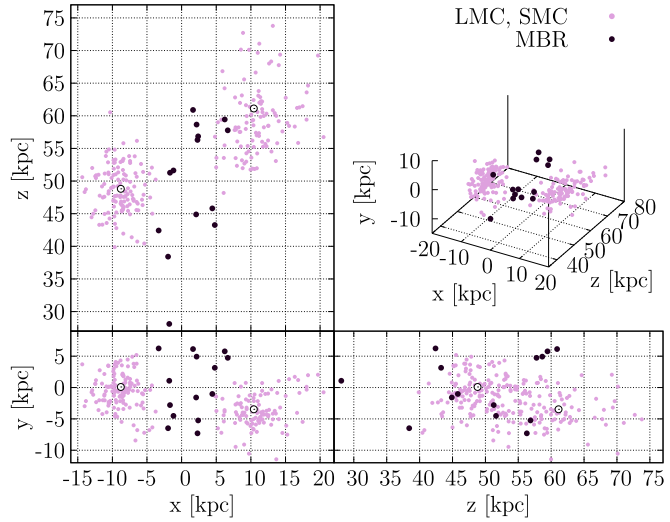


**Figure 8.** Three-dimensional distribution of anomalous Cepheids in the Magellanic System, with the MBR sample marked with darker circles. The map is represented in Cartesian coordinates with the observer located at (0, 0, 0). White circles mark LMC (van der Marel & Kallivayalil 2014; Pietrzyński et al. 2019) and SMC (Stanimirović et al. 2004; Graczyk et al. 2014) centers.

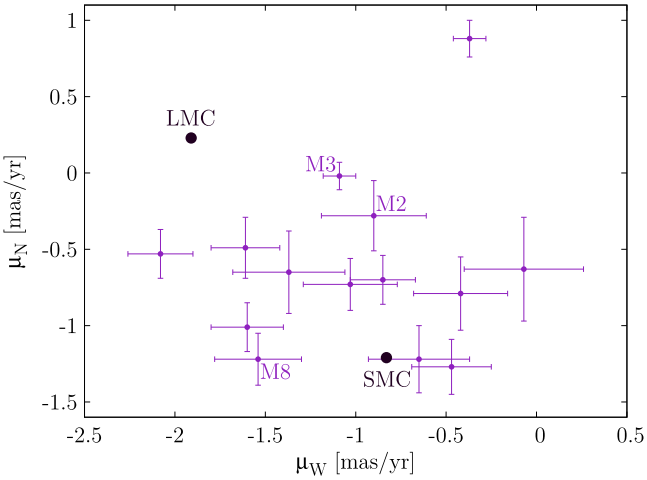


**Figure 9.** PMs of Bridge ACs as compared to the PM of the LMC (Kallivayalil et al. 2013) and SMC (Zivick et al. 2018). Three reclassified Cepheids are shown with their local IDs.

newly added southern extension of the OGLE fields. The parameters of the fits are presented in Table 8 and are consistent with those of Iwanek et al. (2018). There is a slight discrepancy between our results and those of Groenewegen & Jurkovic (2017) and Ripepi et al. (2014) that is probably caused by the latter being based on less numerous samples.

### 5.2. Two- and Three-dimensional Analysis

The on-sky locations of all OGLE ACs along with CCs and T2Cs are presented in Figure 1, where the Bridge sample is highlighted with larger circles. Figure 3 shows a close-up of the central Bridge area. The Cepheid locations are compared to young stars (Skowron et al. 2014) and H I distribution (the Galactic All Sky H I Survey, McClure-Griffiths et al. 2009; Kalberla et al. 2010; Kalberla & Haud 2015). Both plots clearly show that ACs are more spread than CCs and do not form as evident substructures as the latter in any area of the Magellanic System, including the Bridge. In contrary to CCs, ACs do not follow any line or bridge-like connection between the Clouds and do not match either the neutral hydrogen or young population distribution. Nevertheless, this is what we could expect for an older stellar population. For a detailed statistical analysis of the three-dimensional distribution of ACs, see Iwanek et al. (2018).

We were still able to distinguish the Bridge candidates located between the Magellanic Clouds in three dimensions. Figure 8 shows the three-dimensional distribution of ACs in the entire Magellanic System, with the Bridge sample distinguished using larger circles. Although not very numerous, the ACs seem to create a rather smooth connection between the Clouds. However, we cannot state that this connection is bridge-like because these ACs may also be LMC and/or SMC outliers that we also see located in different directions around these galaxies.

### 5.3. Proper Motions

Similarly to CCs, we also used *Gaia* DR2 (Gaia Collaboration et al. 2018) to analyze PMs of our Bridge ACs. Again, we compare results to the LMC and SMC PMs in Figures 9 and 10. ACs follow the general on-sky movement of the entire Magellanic System. Almost all of them fall into the PM range that we would expect for Bridge objects (see Figure 3 from Zivick et al. 2019).

## 6. Reclassified Cepheids

The latest reclassification of four CCs is slightly disputable, as all of these objects have parameters located close to the CC/AC (or CC F/1O) boundary. In Table 9 we compare basic parameters of the four stars before and after the reclassification and list the following: local ID, type, and mode, as well as distance and age before and after the reclassification. The estimates for the latter were already presented in the previous sections. The estimates for before the reclassification were calculated simply including these objects in the appropriate CC or AC sample and using the same technique as for the entire samples that we present in this paper.

The bottom row of Figure 2 shows the four reclassified Cepheids on the PL relations for the entire LMC (left panel) and SMC (right panel) CC and AC samples. The Bridge Cepheid sample is overplotted in each panel using large symbols. Additionally, the reclassified Cepheids are also marked with a star and their local ID. We discuss locations of these objects on the PL diagrams according to all of the presented relations, as these Cepheids may be neither LMC nor SMC members. Thus, their parameters need to be analyzed in a broader context. Note that we do not classify objects based only on their location on the PL diagrams, but we mainly use their light curve (shape and Fourier decomposition parameters; Soszyński et al. 2015a).

M7, which was reclassified from first-overtone CC to fundamental-mode CC, is indeed located much closer to the fundamental mode than first-overtone PL relations. This object is also situated close to the LMC fundamental-mode ACs but at the same time is close to the SMC fundamental-mode CCs. M2, recently reclassified from fundamental-mode CC to fundamental-mode AC, is very close to the LMC fundamental-mode AC PL relation. On the other hand, it is located in between the fundamental-mode CC and AC PL relations for the SMC. M3 is another object reclassified in the same way as M2. M3 is

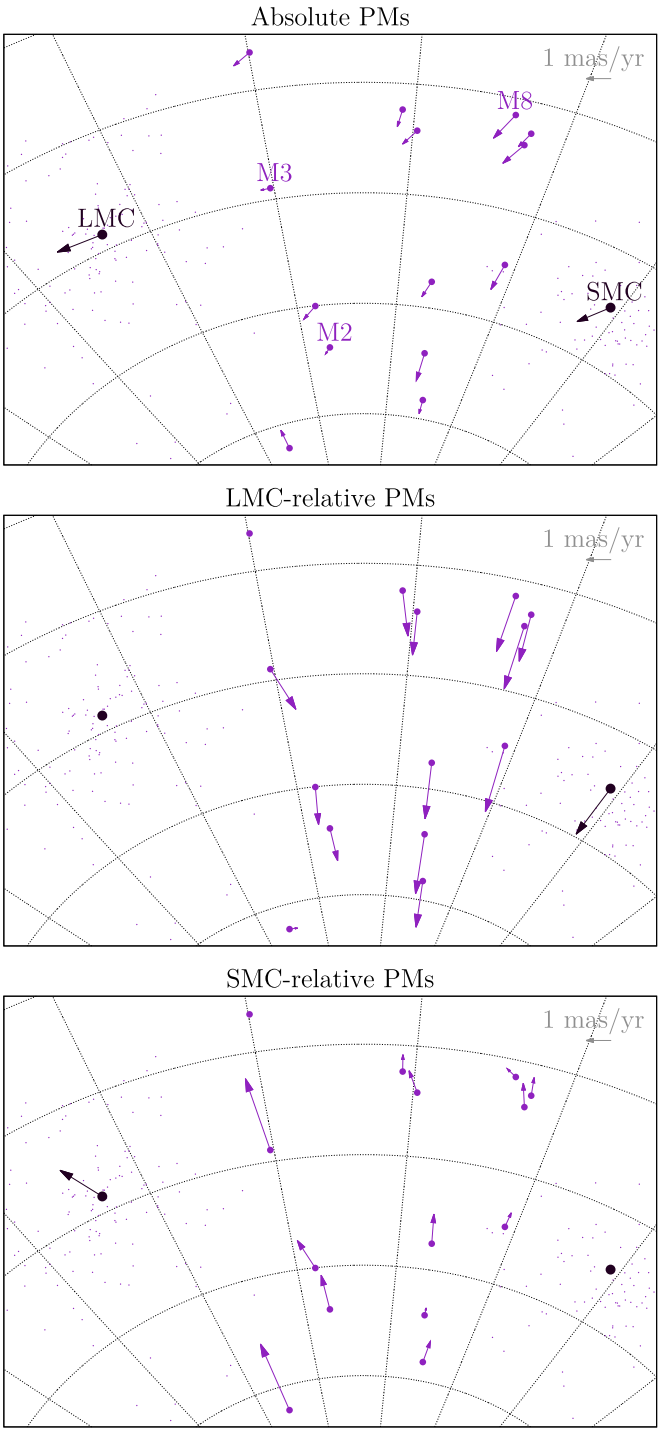


**Figure 10.** PMs of Bridge ACs, as well as LMC (Kallivayalil et al. 2013) and SMC (Zivick et al. 2018), shown as vectors on the sky. The top panel presents absolute PMs, while the middle and bottom panels present the LMC- and SMC-related frame, respectively. We adopted the LMC center of van der Marel & Kallivayalil (2014) and the SMC center of Stanimirović et al. (2004).

situated almost on the fit that we obtained for the first-overtone CCs in the LMC. In fact, it is located quite far from the LMC fundamental-mode PL relation for the CCs, and for the ACs, it is even farther. Compared to the SMC relations, M3 definitely seems to be an outlier from the fundamental-mode PL relations. In the case of M8, which was reclassified from the first-overtone CC to the first-overtone AC, the closest PL relations in the LMC are relations for both types of ACs. This star is located between these relations. When compared to the SMC, M8 is situated close to the first-overtone PL relation for ACs but at the same time is quite close to both PL relations for the CCs.

The reclassification has a significantly changed three-dimensional distribution of Cepheids in the Bridge area, as distances of all reclassified objects have decreased by more than 10 kpc in each case. We show this change in Figure 11, where we plotted projections of a three-dimensional Cartesian distribution of all Cepheids analyzed here (both CCs and ACs), with the Bridge sample highlighted using larger circles. The reclassified objects are marked separately, and the arrows show the change of distances that occurred with the reclassification.

A change of close to or more than 20 kpc has occurred for M2, M7, and M8. If these stars were not reclassified, they would be perfect candidates for Counter Bridge members, as we have already stated in Paper I. Moreover, their ages would match very well the scenario in which they would be formed in situ in this structure. M2 and M8 were reclassified as ACs, and after this change these objects are located in between the Magellanic Clouds, matching very well the three-dimensional distribution of ACs (see Figure 8). M7 is a CC, and even after the reclassification this star could be a Counter Bridge member, though it is now located farther from the center of this structure, and thus this scenario is less plausible (we have discussed M7 location in detail in Section 4.5).

In our Bridge CC sample from Paper I M3 was the closest Cepheid—located even closer than any LMC CC. After the reclassification, this object is located even closer at ∼28 kpc—halfway between the Sun and the Magellanic System. Due to this, M3 was treated as an LMC outlier by our 3$\sigma$-clipping algorithm that we applied to the AC sample. Based on its proximity, we decided to classify this object as Milky Was halo AC.

## 7. *Gaia* DR2 Cepheids in the Bridge

### 7.1. Comparison with OCVS

The *Gaia* DR2 contains a list of variable stars including Cepheids and RR Lyrae stars (Gaia Collaboration et al. 2018; Holl et al. 2018; Clementini et al. 2019). As following Holl et al. (2018), due to the probabilistic and automated nature of the classification process, the *Gaia* DR2 catalog of classical variables is not as complete and pure as the OCVS is (see Table 2 in Holl et al. 2018; Clementini et al. 2019). In this section we revive the *Gaia* DR2 classical pulsators, listed in the `vari_cepheid` table (Gaia Collaboration et al. 2018; Holl et al. 2018), in the MBR area and compare it to the OCVS.

Figure 12 compares on-sky locations of individual Cepheids of different types and modes in the Bridge area. The top row shows OGLE data, while the middle and bottom rows show *Gaia* DR2. The latter shows the DR2 Cepheid sample after the reclassification made by Ripepi et al. (2019). The first three columns show CCs of the following modes, both single- and multimode—fundamental, first-overtone, and both of these together. Based on only these plots, it may seem that *Gaia* DR2 discovered several new CCs that were not present in the virtually complete OGLE Collection of CCs (Soszyński et al. 2017).

Comparing distributions of anomalous Cepheids, both fundamental-mode and first-overtone pulsators, as well as entire samples, the *Gaia* DR2 seems to classify no objects as

**Table 9**
Magellanic Bridge Cepheids: Reclassification

| Loc. ID | Before → After | | | |
|---|---|---|---|---|
| | Type and Mode | $d$ (kpc)[a] | Age (Myr)[b] | |
| M2 | CC F → AC F | 74.07 ± 2.08 → 51.83 ± 1.45 | 233 ± 49 → | NA |
| M3 | CC F → AC F | 39.81 ± 1.11 → 28.18 ± 0.78 | 275 ± 57 → | NA |
| M8 | CC 1O → AC 1O | 80.95 ± 2.23 → 60.05 ± 1.72 | 292 ± 48 → | NA |
| M7 | CC 1O → CC F | 88.83 ± 2.45 → 69.99 ± 1.97 | 151 ± 25 → | 209 ± 44 |

**Notes.**
[a] The distance uncertainty does not include the mean LMC distance uncertainty from Pietrzyński et al. (2019) $d_{\rm LMC} = 49.59 \pm 0.09$ (statistical) $\pm 0.54$ (systematic) kpc.
[b] This age determination was estimated using the period–age relation from Bono et al. (2005) and is available for CCs only.

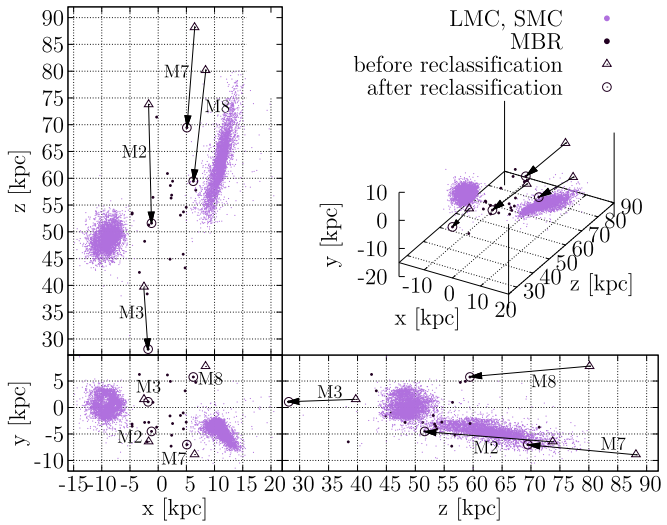


**Figure 11.** Three-dimensional distribution of CCs and ACs in the Magellanic System, with the MBR sample marked with large circles. Additionally, locations of four reclassified Cepheids are highlighted with different markers. Arrows show the direction of changes in locations. Labels show local IDs of these objects (see Table 9). The map is represented in the Cartesian coordinates with the observer located at (0, 0, 0).

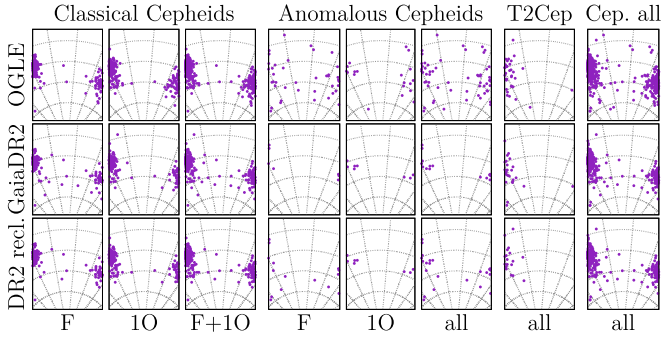


**Figure 12.** Comparison of OGLE (top row) and *Gaia* DR2 (middle and bottom rows) Cepheids in the Magellanic Bridge area. The bottom row shows the DR2 sample after the reclassification made by Ripepi et al. (2019). It may seem that *Gaia* DR2 discovered more CCs in the Bridge area than contained in the nearly complete OCVS. However, a comparison of different panels leads to a conclusion that many of the ACs were classified in DR2 as CCs. Finally, the OCVS contains several more Cepheids in the Bridge area than DR2.

anomalous Cepheids in the Bridge. At the same time, the OCVS contains many ACs in between the Magellanic Clouds. This leads to a conclusion that many ACs were classified as CCs in DR2. This is probably due to different classification methods used in both cases (i.e., see reclassification of the Milky Way Cepheids from *Gaia* DR2 in Ripepi et al. 2019). It is very similar for T2Cs, though neither OGLE nor *Gaia* DR2 classifies any objects of this type in the central Bridge area. A comparison of all of the Cepheids between the Magellanic Clouds reveals that the *Gaia* DR2 has incorrectly cataloged a number of objects in the Bridge area.

We compared the OCVS and *Gaia* DR2 Cepheid samples in numbers. For the cross-match we selected a DR2 sample covering the entire OGLE fields in the Magellanic System (see Figure 1). We use the OCVS sample containing the latest updates and corrections as described in Section 2.1. Out of 10,140 Cepheids included in the OGLE Collection in the Magellanic System (9532 CCs, 268 ACs, 340 T2Cs), 7490 objects were found in the *Gaia* DR2 Cepheid sample. Thus, when comparing to the virtually complete OGLE Collection of Cepheids, the *Gaia* DR2 completeness is on a level of 73.9%, which is consistent with Table 2 in Holl et al. (2018). High completeness is not surprising, as the OCVS Cepheid data set from the Magellanic Clouds was a training set for the *Gaia* Cepheid detection algorithms. In other areas of the sky, the *Gaia* DR2 Cepheid sample completeness is significantly lower, i.e., Udalski et al. (2018) showed that in the Milky Way disk and bulge area it is on a level of 9.1%.

We additionally compared the *Gaia* DR2 detections in the region designed as MBR in OGLE-IV fields (Figure 18 in Udalski et al. 2015). A total of 30 *Gaia* DR2 Cepheids are located in the OGLE MBR field footprint; 29 were confirmed in the OGLE Collection as genuine Cepheids, and the one lacking object is likely an eclipsing star. A total of 59 Cepheids in the OGLE Collection (CCs, ACs, and T2Cs) lie in the OGLE MBR fields. Thus, the completeness of the *Gaia* DR2 in this region is $29/59 \simeq 49\%$.

## 8. Conclusions

In this paper, which is the third in a series of analyzing the three-dimensional structure of the Magellanic System, we present an updated detailed analysis of Cepheids in the MBR. We use data from the OGLE project—released parts of the OCVS (Soszyński et al. 2015b, 2017, 2018, 2019). The collection was recently updated: seven Cepheids were added, and four were reclassified. We present a thorough study of classical and anomalous Cepheid Bridge samples using very precise OGLE photometry. We note that we did not classify any T2C as an MBR member owing to their absence in this area.

Similarly to Paper I, our basic method of calculating distances relies on fitting PL relations using the Wesenheit $W_{I,V-I}$ index to the entire LMC sample. Then, we estimate the

individual distance of each Cepheid relative to the LMC mean distance and the LMC fit. Based on three-dimensional coordinates and on-sky locations of stars in relation to the LMC and SMC entire samples, we selected our Bridge samples.

The updated Bridge CC sample contains 10 objects. As compared to the Paper I sample, we removed three objects (M2, M3, and M8, which were reclassified as ACs) and added four objects (M10, added by Soszyński et al. 2017, and M11–M13). On-sky locations of the CC MBR sample match very well the H I density contours and the young stars' distribution. Only two Cepheids, namely, M7 and M10, are located slightly offset, though still well within the densest regions. The CCs add to the overall distribution of young stars in the Bridge area.

In three dimensions, 8 out of 10 objects from the CC sample form a bridge-like connection between the Magellanic Clouds. Four out of these eight are located close to the LMC (M12 and M13) or SMC (M9 and M11). Two that do not form the bridge-like connection, namely, M1 and M7, are located slightly farther than the main sample; thus, they may constitute a Counter Bridge. However, they may also be genuine MBR members. Further study is needed to test this. We also analyzed different methods of obtaining distances and conclude that the adopted reddening law does not influence results much and the reddening toward the Bridge is low. Moreover, the individual dereddening method used by, e.g., Haschke et al. (2012a, 2012b) seems to be inappropriate in this case.

From 5 up to 8 out of 10 Bridge CCs have ages of less than 300 Myr (as based on the period–age relations from Bono et al. 2005; Anderson et al. 2016). This agrees with a hypothesis that some of the Bridge objects may have been formed in situ after the last encounter of the Magellanic Clouds. The two youngest CCs have ages less than 60 Myr. The two oldest CCs can be LMC or SMC members. Moreover, their periods are shorter than 1 day; thus, their age estimate may not be appropriate, as the models do not predict ages of such short-period pulsators.

Our Bridge AC sample consists of 13 objects. Their on-sky locations do not match H I or young star density contours. AC distribution is very spread out in both two and three dimensions. However, they form a rather smooth connection between the Magellanic Clouds. But we also cannot state that this connection is bridge-like, as these stars may also be LMC/SMC outliers.

We also tested *Gaia* DR2 Cepheids' on-sky distribution in the Bridge area. DR2 contains more CCs in the MBR than the OCVS. However, DR2 does not include virtually any AC in between the Magellanic Clouds. This is explained by a different classification process, where many ACs are classified as CCs in DR2. A comparison of all types of Cepheids shows that the OCVS has more objects in the MBR and thus is definitely more complete.

We present a complementing study of older classical pulsators in the MBR—RR Lyrae stars—in a closely following Paper IV.

A.M.J.-D. is supported by the Polish Ministry of Science and Higher Education under "Diamond Grant" No. DI2013 014843 and by the Deutsche Forschungsgemeinschaft (DFG, German Research Foundation)—Project-ID 138713538—SFB 881 ("The Milky Way System," subproject A03). The OGLE project has received funding from the National Science Centre, Poland, grant MAESTRO 2014/14/A/ST9/00121 to A.U.

We would like to thank all of those whose remarks and comments inspired us and helped to make this work more valuable, especially the anonymous referee. In particular, we would also like to thank Richard Anderson, Abhijit Saha, Vasily Belokurov, Anthony Brown, Laurent Eyer, Martin Groenewegen, Vincenzo Ripepi, Radosław Smolec, Martino Romaniello, and Krzysztof Stanek.

This research was supported by the Munich Institute for Astro- and Particle Physics (MIAPP) of the DFG cluster of excellence "Origin and Structure of the Universe," as it benefited from the MIAPP program "The Extragalactic Distance Scale in the *Gaia* Era," as well as the International Max Planck Research School (IMPRS) Summer School on "*Gaia* Data and Science 2018."

This work has made use of data from the European Space Agency (ESA) mission *Gaia* (https://www.cosmos.esa.int/gaia), processed by the *Gaia* Data Processing and Analysis Consortium (DPAC, https://www.cosmos.esa.int/web/gaia/dpac/consortium). Funding for the DPAC has been provided by national institutions, in particular the institutions participating in the *Gaia* Multilateral Agreement.

## ORCID iDs

Anna M. Jacyszyn-Dobrzeniecka https://orcid.org/0000-0002-5649-536X
Igor Soszyński https://orcid.org/0000-0002-7777-0842
Jan Skowron https://orcid.org/0000-0002-2335-1730
Przemek Mróz https://orcid.org/0000-0001-7016-1692
Patryk Iwanek https://orcid.org/0000-0002-6212-7221
Paweł Pietrukowicz https://orcid.org/0000-0002-2339-5899
Radosław Poleski https://orcid.org/0000-0002-9245-6368
Szymon Kozłowski https://orcid.org/0000-0003-4084-880X
Krzysztof Ulaczyk https://orcid.org/0000-0001-6364-408X

## References

Alcock, C., Allsman, R. A., Axelrod, T. S., et al. 1995, AJ, 109, 1653
Anderson, R. I., Saio, H., Ekström, S., Georgy, C., & Meynet, G. 2016, A&A, 591, A8
Bagheri, G., Cioni, M.-R. L., & Napiwotzki, R. 2013, A&A, 551, A78
Barger, K. A., Haffner, L. M., & Bland-Hawthorn, J. 2013, ApJ, 771, 132
Belokurov, V., Erkal, D., Deason, A. J., et al. 2017, MNRAS, 466, 4711
Besla, G., Kallivayalil, N., Hernquist, L., et al. 2012, MNRAS, 421, 2109
Bhardwaj, A., Ngeow, C.-C., Kanbur, S. M., & Singh, H. P. 2016, MNRAS, 458, 3705
Bica, E. L. D., Santiago, B., Bonatto, C., et al. 2015, MNRAS, 453, 3190
Bica, E. L. D., & Schmitt, H. R. 1995, ApJS, 101, 41
Bono, G., Marconi, M., Cassisi, S., et al. 2005, ApJ, 621, 966
Carrera, R., Conn, B. C., Noël, N. E. D., et al. 2017, MNRAS, 471, 4571
Clementini, G., Ripepi, V., Molinaro, R., et al. 2019, A&A, 622, A60
Deason, A. J., Belokurov, V., Erkal, D., Koposov, S. E., & Mackey, D. 2017, MNRAS, 467, 2636
Deb, S., Ngeow, C.-C., Kanbur, S. M., et al. 2018, MNRAS, 478, 2526
Demers, S., & Battinelli, P. 1998, AJ, 115, 154
Diaz, J. D., & Bekki, K. 2012, ApJ, 750, 36
D'Onghia, E., & Fox, A. J. 2016, ARA&A, 54, 363
Fiorentino, G., & Monelli, M. 2012, A&A, 540, A102
Fouqué, P., Arriagada, P., Storm, J., et al. 2007, A&A, 476, 73
Gaia Collaboration, Brown, A. G. A., et al. 2018, A&A, 616, A1
Gallenne, A., Kervella, P., Mérand, A., et al. 2017, A&A, 608, A18
Gardiner, L. T., & Noguchi, M. 1996, MNRAS, 278, 191
Gardiner, L. T., Sawa, T., & Fujimoto, M. 1994, MNRAS, 266, 567
Gieren, W., Storm, J., Konorski, P., et al. 2018, A&A, 620, 99
Graczyk, D., Pietrzyński, G., Thompson, I. B., et al. 2014, ApJ, 780, 59
Groenewegen, M. A. T., & Jurkovic, M. I. 2017, A&A, 604, A29
Groenewegen, M. A. T., & Oudmaijer, R. D. 2000, A&A, 356, 849
Guglielmo, M., Lewis, G. F., & Bland-Hawthorn, J. 2014, MNRAS, 444, 1759

Harris, J. 2007, ApJ, 658, 345
Haschke, R., Grebel, E. K., & Duffau, S. 2012a, AJ, 144, 106
Haschke, R., Grebel, E. K., & Duffau, S. 2012b, AJ, 144, 107
Hindman, J. V., Kerr, F. J., & McGee, R. X. 1963, AuJPh, 16, 570
Holl, B., Audard, M., Nienartowicz, K., et al. 2018, A&A, 618, A30
Indu, G., & Subramaniam, A. 2015, A&A, 573, A136
Inno, L., Bono, G., Matsunaga, N., et al. 2016, ApJ, 832, 176
Inno, L., Matsunaga, N., Bono, G., et al. 2013, ApJ, 764, 84
Irwin, M. J., Kunkel, W. E., & Demers, S. 1985, Natur, 318, 160
Iwanek, P., Soszyński, I., Skowron, D., et al. 2018, AcA, 68, 213
Jacyszyn-Dobrzeniecka, A. M., Kruszyńska, K., Mróz, P., et al. 2020, ApJ, 889, 26
Jacyszyn-Dobrzeniecka, A. M., Skowron, D. M., Mróz, P., et al. 2016, AcA, 66, 149
Jacyszyn-Dobrzeniecka, A. M., Skowron, D. M., Mróz, P., et al. 2017, AcA, 67, 1
Kalberla, P. M. W., & Haud, U. 2015, A&A, 578, A78
Kalberla, P. M. W., McClure-Griffiths, N. M., Pisano, D. J., et al. 2010, A&A, 512, A14
Kallivayalil, N., van der Marel, R. P., Besla, G., Anderson, J., & Alcock, C. 2013, ApJ, 764, 161
Kochanek, C. S., Schappee, B. J., Stanek, K. Z., et al. 2017, PASP, 129, 104502
Koposov, S. E., Walker, M. G., Belokurov, V., et al. 2018, MNRAS, 479, 5343
Lehner, N., Howk, J. C., Keenan, F. P., & Smoker, J. V. 2008, ApJ, 678, 219
Lemasle, B., François, B., Genovali, K., et al. 2013, A&A, 558, A31
Mackey, A. D., Koposov, S. E., Da Costa, G. S., et al. 2017, MNRAS, 472, 2975
Madore, B. F. 1982, ApJ, 253, 575
Madore, B. F., Freedman, W. L., & Moak, S. 2017, ApJ, 842, 42
McClure-Griffiths, N. M., Pisano, D. J., Calabretta, M. R., et al. 2009, ApJS, 181, 398
Misawa, T., Charlton, J. C., Kobulnicky, H. A., Wakker, B. P., & Bland-Hawthorn, J. 2009, ApJ, 695, 1382
Moretti, M. I., Clementini, G., Muraveva, T., et al. 2014, MNRAS, 437, 2702
Ngeow, C.-C. 2012, ApJ, 747, 50
Ngeow, C.-C., Sarkar, S., Bhardwaj, A., Kanbur, S. M., & Singh, H. P. 2015, ApJ, 813, 57
Nikolaev, S., Drake, A. J., Keller, S. C., et al. 2004, ApJ, 601, 260
Noël, N. E. D., Conn, B. C., Carrera, R., et al. 2013, ApJ, 768, 109
Noël, N. E. D., Conn, B. C., Read, I. J., et al. 2015, MNRAS, 452, 4222
Oey, M. S., Dorigo Jones, J., Castro, N., et al. 2018, ApJL, 867, L8
Pietrzyński, G., Graczyk, D., Gallenne, A., et al. 2019, Natur, 567, 200
Ploeckinger, S., Hensler, G., Recchi, S., Mitchell, N., & Kroupa, P. 2014, MNRAS, 437, 3980
Ploeckinger, S., Recchi, S., Hensler, G., & Kroupa, P. 2015, MNRAS, 447, 2512
Ploeckinger, S., Sharma, K., Schaye, J., et al. 2018, MNRAS, 474, 580
Ripepi, V., Cioni, M.-R., Moretti, M. I., et al. 2017, MNRAS, 472, 808
Ripepi, V., Marconi, M., Moretti, M. I., et al. 2014, MNRAS, 437, 2307
Ripepi, V., Molinaro, R., Musella, I., et al. 2019, A&A, 625, A14
Růžička, A., Theis, C., & Palouš, J. 2010, ApJ, 725, 369
Sandage, A., Tammann, G. A., & Reindl, B. 2004, A&A, 424, 43
Sandage, A., Tammann, G. A., & Reindl, B. 2009, A&A, 493, 471
Schappee, B. J., Prieto, J. L., Grupe, D., et al. 2014, ApJ, 788, 48
Schlegel, D. J., Finkbeiner, D., & Davis, M. 1998, ApJ, 500, 525
Scowcroft, V., Freedman, W. L., Madore, B. F., et al. 2016, ApJ, 816, 49
Shapley, H. 1940, BHarO, 914, 8
Skowron, D. M., Jacyszyn, A. M., Udalski, A., et al. 2014, ApJ, 795, 108
Soszyński, I., Poleski, R., Udalski, A., et al. 2008, AcA, 58, 163
Soszyński, I., Udalski, A., Szymański, M. K., et al. 2015a, AcA, 65, 233
Soszyński, I., Udalski, A., Szymański, M. K., et al. 2015b, AcA, 65, 297
Soszyński, I., Udalski, A., Szymański, M. K., et al. 2017, AcA, 67, 103
Soszyński, I., Udalski, A., Szymański, M. K., et al. 2018, AcA, 68, 89
Soszyński, I., Udalski, A., Szymański, M. K., et al. 2019, AcA, 69, 87
Stanimirović, S., Staveley-Smith, L., & Jones, P. A. 2004, ApJ, 604, 176
Storm, J., Gieren, W., Fouqué, P., et al. 2011, A&A, 534, A95
Sziládi, K., Vinkó, J., Poretti, E., Szabados, L., & Kun, M. 2007, A&A, 473, 579
Sziládi, K., Vinkó, J., & Szabados, L. 2018, AcA, 68, 111
Tammann, G. A., Sandage, A., & Reindl, B. 2003, A&A, 404, 423
Tammann, G. A., Sandage, A., & Reindl, B. 2008, ApJ, 679, 52
Udalski, A. 2003, ApJ, 590, 284
Udalski, A., Soszyński, I., Pietrukowicz, P., et al. 2018, AcA, 68, 315
Udalski, A., Szymański, M. K., Kubiak, M., et al. 1999, AcA, 49, 201
Udalski, A., Szymański, M. K., & Szymański, G. 2015, AcA, 65, 1
van der Marel, R. P., & Kallivayalil, N. 2014, ApJ, 781, 121
Wagner-Kaiser, R., & Sarajedini, A. 2017, MNRAS, 466, 4138
Zivick, P., Kallivayalil, N., Besla, G., et al. 2019, ApJ, 874, 78
Zivick, P., Kallivayalil, N., van der Marel, R. P., et al. 2018, ApJ, 864, 55